mouse by the standard procedure. Mice were screened for the transgene by PCR using *ganp* 1–5′ primer (5′-TCCCGCCTTCCAGCTGTGAC-3′) and *ganp* 1–3′ primer (5′-GTGCTGCTGTGTTAT GTCCT-3′) and Southern blot analysis using *ganp* probe A (1143–2193 nt) of tail genomic DNAs. The *Ganp*^{Tg} mice that express 1.5- to 2.0-fold increase of *ganp* gene grew normally under specific pathogen-free condition and were immunized with Ags. *Ganp* transcripts were detected by two primers (*ganp* 1–5′ and *ganp* 1–3′) in comparison with *β-actin* control (5). All mice were maintained in the Center for Animal Resources and Development (Kumamoto University, Kumamoto, Japan).

Flow cytometric analysis

Single-cell suspensions from lymphoid organs were stained with each biotin-labeled mAb in combination with FITC-conjugated streptavidin (Amersham Biosciences) and PE-conjugated mAbs. Lymphoid cells were analyzed by FACSCalibur (BD Biosciences) using CellQuest software.

In vitro proliferation assay

Purified B cells were cultured for 48 h at a density of 2×10^5 cells/well in 96-well microtiter plates in RPMI 1640 medium containing 10% heat-inactivated FCS (JRH Biosciences), 2 mM L-glutamine, and 5×10^{-5} M 2-ME. The cells stimulated with or without various mitogenic stimulants were pulsed with 0.2 μCi/well of [^{3}H]thymidine (ICN Pharmaceuticals) for 16 h before harvesting, and the incorporated radioactivity was measured by scintillation counter. Stimulatory reagents were affinity-purified goat anti-mouse μ-chain-specific Ab ($F(ab')_2$, 10 μg/ml; ICN Pharmaceuticals), rat anti-mouse CD40 mAb (LB429, 10 μg/ml) (4), and LPS (10 μg/ml; Sigma-Aldrich).

Immunohistochemistry

The 8-μm sections of spleen from SRBC-immunized mice were lightly fixed with acetone. Slides were blocked with 3% BSA in PBS-Tween 20

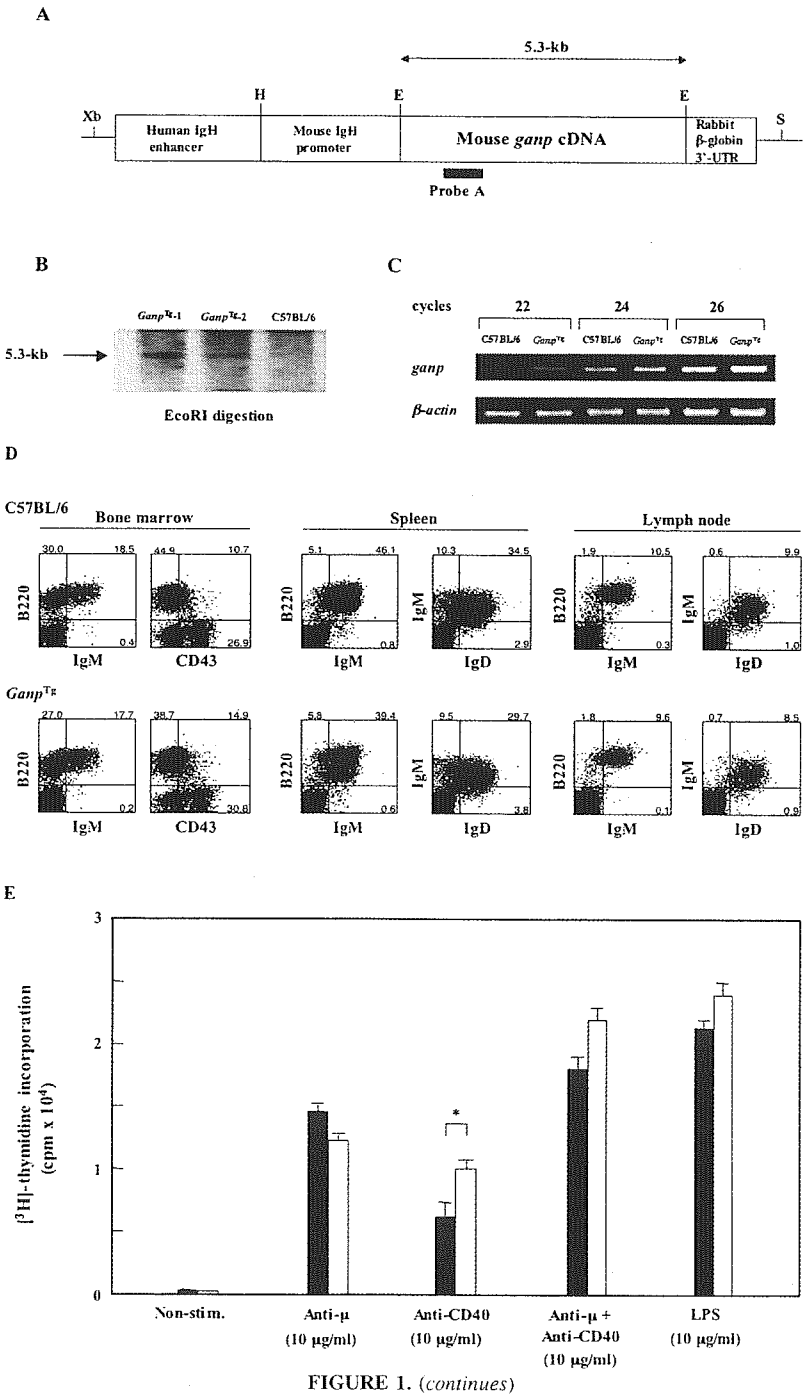

FIGURE 1. Generation of transgenic mice that overexpress the *ganp* gene in B cells. *A*, A schematic diagram of construct for *Ganp*^{Tg} under the human Ig enhancer, mouse Ig promoter, and followed by rabbit β-globin 3′-untranslated region (UTR). The construct contains restriction enzyme sites: Xb, *Xba*I; H, *Hin*dIII; E, *Eco*RI; and S, *Sal*I. The probe for Southern blot analysis (probe A) is indicated. *B*, Detection of the *ganp* transgene by Southern blot analysis. Southern blot analysis with *Eco*RI-digested genomic DNAs of *Ganp*^{Tg} displayed a 5.3-kb band hybridized with probe A. *C*, Up-regulation of *ganp* transcripts in B cells from *Ganp*^{Tg}. Semiquantitative PCR was performed using the primers *ganp* 1–5′ and *ganp* 1–3′, in comparison with *β-actin* transcripts. From densitometer analysis, *ganp* transcripts in B cells from *Ganp*^{Tg} showed an 80% increase in comparison with C57BL/6 mice. *D*, Flow cytometric analysis. Bone marrow, spleen, and lymph node cells from 8-wk-old C57BL/6 and *Ganp*^{Tg} were analyzed with indicated markers. *E*, In vitro proliferation assay of purified B cells from *Ganp*^{Tg}. [^{3}H]Thymidine incorporation was measured in the presence or absence of B cell mitogenic stimulants in C57BL/6 mice (■) and *Ganp*^{Tg} mice (□). The representative data are shown from four independent experiments. *, $p < 0.05$. *F*, Kinetics of GC formation after TD-Ag in *Ganp*^{Tg}. C57BL/6 and *Ganp*^{Tg} mice were immunized by SRBC. At day 10 or day 14, the sections were doubly immunostained with peanut agglutinin (brown) and IgD (blue). Arrows indicate GCs. *G*, T cell-independent Ag (type II)-specific or TD-Ag-specific immune responses in *Ganp*^{Tg}. Sera from mice immunized with TNP-Ficoll or TNP-KLH were collected at day 14. TNP-specific Ab titers were measured by ELISA. C57BL/6 mice (●) and *Ganp*^{Tg} mice (○) are indicated. *H*, Relative affinity of serum Abs in *Ganp*^{Tg}. Sera from C57BL/6 and *Ganp*^{Tg} mice immunized with NP-CG were collected at days 14 and 28. The NP_2 to NP_{17} ratios of anti-NP IgG1 were measured by ELISA. *I*, W33L mutation of $V_H186.2$ transcripts from C57BL/6 and *Ganp*^{Tg} mice. Mice were i.p. immunized by 20 μg of alum-precipitated NP-CG. $V_H186.2$ transcripts of γ1-isotype were amplified by RT-PCR and cloned into pBluescript vector for sequencing. The calculated percentage from sequence data was shown in C57BL/6 (■) and *Ganp*^{Tg} (□) mice. *, $p < 0.05$.

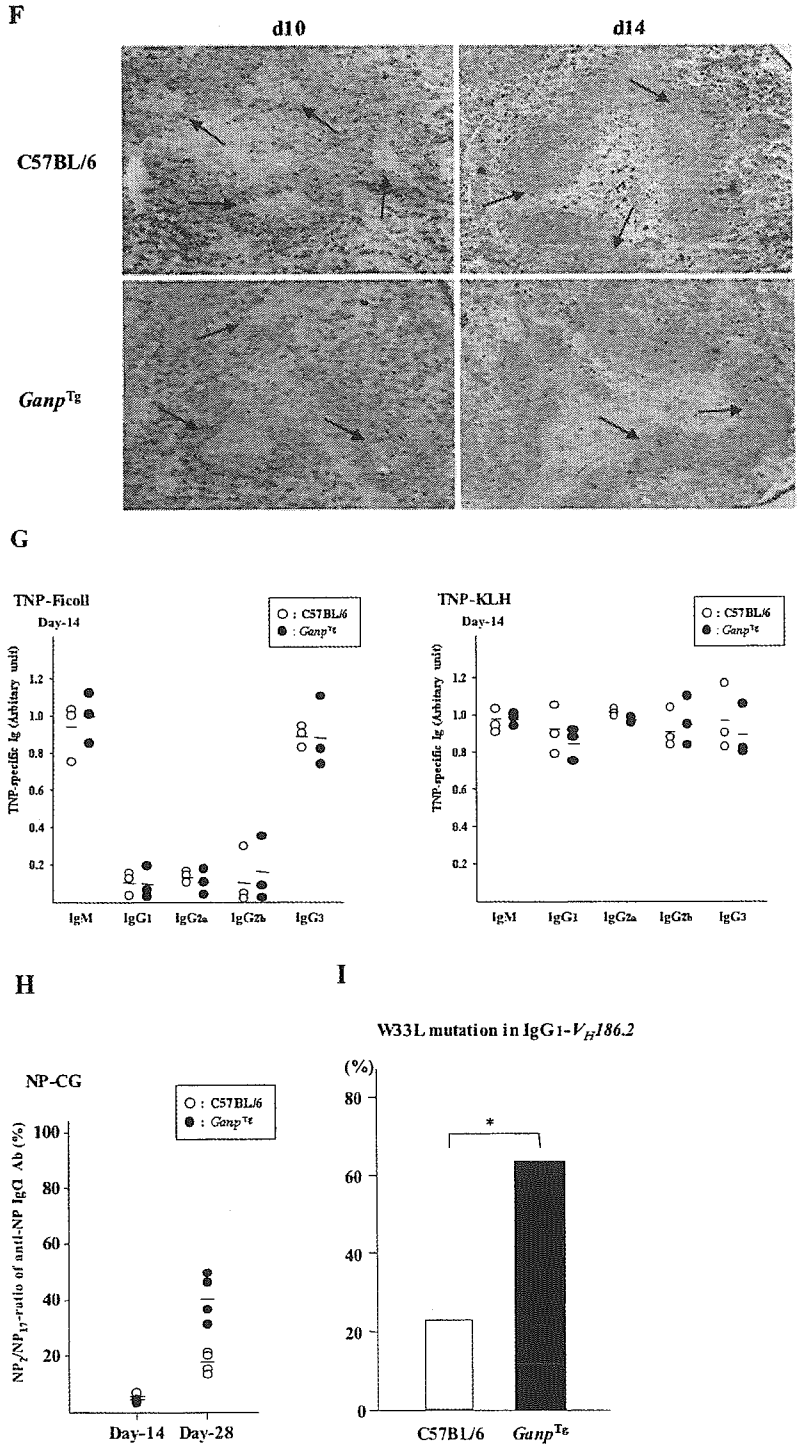

FIGURE 1. *continued.*

and incubated with anti-IgD mAb in combination with alkaline phosphatase-conjugated anti-rat IgG (ICN Pharmaceuticals). The first development step was conducted with Vector Blue kit (Vector Laboratories). For second staining, slides were incubated with biotin-conjugated peanut agglutinin (Vector Laboratories) in combination with HRP-conjugated streptavidin (Kirkegaard & Perry Laboratories), followed by 3,3′-diaminobenzidine tetrahydrochloride (Dojindo). After fixation with 1% glutaraldehyde in PBS, mounting was done by Aquatex (Merck).

Ag and immunization

2,4,6-Trinitrophenyl (TNP)-keyhole limpet hemocyanin (KLH), TNP-Ficoll, and NP_{28}-CG were purchased from Biosearch Technologies. From 20 to 100 μg of TNP-KLH and NP-CG precipitated by alum (Pierce), or 25 μg of TNP-Ficoll dissolved in PBS was injected i.p. into C57BL/6 and *Ganp*^{Tg} mice.

Measurement of Ag-specific Ab production

Five micrograms per well of TNP-BSA (Biosearch Technologies) were coated on ELISA plate, blocked with 3% BSA in PBS, and incubated with the serial-diluted sera obtained at day 14 after Ag immunization. After washing with PBS-0.1% Tween 20, the wells were incubated with biotin-conjugated isotype-specific mAb in combination with alkaline phosphatase-conjugated streptavidin (Southern Biotechnology Associates). The development was performed in the presence of substrate.

Sequence analysis of V_H186.2 gene

The *Ganp*^{Tg} mice were immunized with alum-precipitated NP-CG once as described (5). After 28 days, the spleen B cells were purified, and the total

Table I. *Affinity of the anti-NP mAb measured by BIAcore sensorgram*

mAb	H Chain	L Chain	V_H Usage	K_D, M[a]
Ganp^{Tg}				
NP-G2-6	γ1	κ	V_H 7183 family	7.05×10^{-8}
NP-G2-9	γ1	κ	V_H 7183 family	3.24×10^{-8}
NP-G2-12	γ1	λ	V_H 186.2	4.92×10^{-8}
NP-G2-14	γ1	κ	V_H 186.2	2.51×10^{-8}
NP-G2-16	γ2b	λ	V_H 186.2	1.10×10^{-7}
NP-G2-15	γ1	λ	V_H 186.2	4.12×10^{-8}
NP-G-2E4	γ2b	λ	V_H 186.2	1.57×10^{-9}
C57BL/6				
NP-W2-7	γ1	λ	V_H 186.2	1.51×10^{-7}
NP-W1-116	γ2a	λ	V_H 186.2	1.00×10^{-8}
NP-W-1B9	γ2b	λ	V_H 186.2	1.24×10^{-8}
NP-W-2D8	γ2b	λ	V_H 186.2	2.74×10^{-8}

[a] K_D was calculated using BIAcore sensorgram as described in *Materials and Methods*.

RNA was used for RT-PCR analysis with the sequence primers for IgG1-V_H*186.2* and the sequences were compared with those of C57BL/6.

Establishment of mAbs

Ag immunization was conducted with CFA as a primary immunization and then followed by boosting with IFA (4). For anti-NP-specific mAbs, NP_{28}-CG emulsified in CFA was injected i.p. and boosted after 2 wk with IFA. The mice with higher serum Ab titers were further immunized, and 3 days later, the spleen cells were obtained for cell fusion by polyethylene glycol method with mouse myeloma cell line X63 under the standard procedure (4). The fused cells were selected with hypoxanthine/aminopterin/thymidine medium on the microculture plates at the concentration of 2×10^4 cells/well with IL-6 (5 U/ml). For preparation of mAbs against the epitope of HIV-1, the peptide of the CNNTRKSIRIQRGPGRAFVYIGKI was prepared based on the amino acid sequence of the V3 loop of gp120 region of NL4-3 HIV-1 strain (prototype X4; T cell tropic) and conjugated with KLH (Merck). Sera of immunized mice were measured by ELISA using the plates coated with the HIV-1 peptide conjugated with BSA.

ELISA screening

For anti-NP mAbs, supernatants of individual wells were divided into two aliquots (each 50 μl) and measured by the differential ELISA method with two different Ag-coating as NP_2-BSA and NP_{17}-BSA (Biosearch Technologies) under the standard procedure. The mAbs binding to the Ags were captured with protein A-peroxidase (Amersham Biosciences) with the substrate (Bio-Rad). The positive signals with NP_2-BSA plates were selected in comparison with NP_{17}-BSA plates. The mAbs showing little difference (NP_2-BSA/NP_{17}-BSA > 0.5) between the two plates were cloned by limiting dilution method. Then, the positive clones were expanded for large scale to purify the mAbs in the serum-free medium (Invitrogen Life Technologies) and the mAbs were purified through protein G-Sepharose column chromatography (Amersham Biosciences) and the protein concentrations were determined by Bradford assay kit (Bio-Rad). The purities of the samples were examined by SDS-PAGE and the protein staining with Coomassie brilliant blue. The isotypes of H chain and L chain in all mAbs were determined by Isotyping kit (Dainippon Pharmaceuticals).

BIAcore assay

Affinity of the mAbs was determined by the BIAcore assay (7). The on and off rate constants (k_{on} and k_{off}) for binding of the mAbs to NP or HIV-1 V3 loop peptide were determined by BIAcore system (Biacore International). The carboxyl-methylated dextran surface of the sensor chip was activated with EDC (*N*-ethyl-*N'*-(3-dimethylaminopropyl)carbodiimide) and NHS (*N*-hydroxysuccinimide) (8). V3 loop peptide was immobilized through the free thiol group of a cysteine residue that was deliberately placed at the N terminus, by injection of 35 μl of a 20 μg/ml solution in 10 mM MES buffer (pH 6) to the EDC-NHS-activated surface that had been reacted with 2-(2-pyridinyldithio)ethaneamine. The excess disulfide groups were deactivated by the addition of cysteine. The mAbs were diluted in 10 mM HEPES (pH 7.4), 150 mM NaCl, 3.4 mM EDTA, and 0.05% (v/v) BIAcore surfactant P20 and injected over the immobilized Ag at a flow rate of 5 μl/min. The association was monitored by the increase of the refractive index of the sensor chip surface per unit time. The dissociations of the mAbs were monitored after the end of the association phase with a flow rate of 50 μl/min. Kinetic rate constants were calculated from the collected data using the Pharmacia Kinetics Evaluation software (9). The k_{on} was determined by measuring the rate of binding to the Ag at different protein concentrations.

DNA sequencing

The DNA fragments corresponding to the rearranged V_H regions were amplified using Pfu-Turbo (Stratagene) from the genomic DNA. The oligonucleotide primers are as follows (10, 11): V_H186.2 forward, 5'-CTGAC CCATGTCCCTTCTTCTCCAGCAGG-3'; V_H7183 forward, 5'-GCA GCTGGTGGAGTCTGG-3'; J_H4-3, 5'-CTCTCAGCCGGCTCCCTCA GGG-3'; Vλ1 forward, 5'-TGCTGACCAATATTGAAAAG-3'; Jλ1 reverse, 5'-AGCACCTCAAGTCTTGGAGAG-3'. For rearranged *V* κ-chain genes, the cDNA fragments were amplified using the primers designed as follows (12): V κ-Ox1 forward, 5'-ATGGATTTTCAAGTGCAGATTTTCA-3'; Vκ-21B forward, 5'-ATGGAGTCAGACACACTCCTGCTAT-3'; and Cκ reverse, 5'-TGGGAAGATGGATACAGTTGGTGCA-3'. Amplification of Cμ region was conducted with the primers: Cμ-Ex1 forward, 5'-AGTCAGTCCTTCCCAAATGTCTTCCC-3' and Cμ-Ex3 reverse, 5'-TGAAGGTTAGGATGTCTGTGGAGGG-3'. The amplified DNA fragments cloned into blunt-ended pBluescript were sequenced.

In vitro binding assay to NL4-3 envelope

293T cells were transfected with pLP-IRES2 enhanced GFP (BD Clontech) or pLP-NL4-3 envelope enhanced GFP using Effectene Transfection Reagent (Qiagen). After 36 h, cells were harvested, incubated with each anti-HIV-1 mAb in combination with allophycocyanin-conjugated goat anti-mouse IgG Ab (BD Pharmingen), and analyzed in comparison with GFP expression by FACSCalibur. The anti-CD19 mAb was purchased from BD Biosciences.

Neutralization activity assay

HIV-1 strain NL4-3 (prototype X4; T cell tropic) was propagated in PM1 cells in RPMI 1640 medium with 10% (v/v) heat-inactivated FCS, and the cell-free supernatant was collected and stored as virus stocks at −80°C. The chemiluminescent assay (Galacto-Star; Applied Biosystems) for β-galactosidase released from the HeLa-CD4$^+$/long terminal repeat (LTR)-β-galactosidase/CCR5 (MAGI/CCR5) cells were conducted as previously described (13). Tissue culture-effective dose $(TCID)_{50}$ of virus stock was predetermined with MAGI/CCR5 cells by the method of Reed and Muench (14). For the assay of neutralizing activity against HIV-1 infection, MAGI/CCR5 cells were plated in 96-well microtiter plates at a density of 1×10^4 cells/well, and on the next day, the cells were incubated with 50 μl of each mAb and 50 μl of HIV-1 solution (500 $TCID_{50}$) for 30 min at 37°C in combination with 10 μg/ml DEAE-dextran (Amersham Biosciences) in a triplicate assay. After 48 h, we measured the β-galactosidase activity for 1 s using the Galacto-Star system according to the manufacturer's protocol and showed results as percentages of the negative control.

Results

Establishment of Ganp^{Tg} *mice*

Ganp^{Tg} mice were established under control by human Ig enhancer and mouse Ig promoter in C57BL/6 background (Fig. 1, *A* and *B*), and the adult mice showed an increase of *ganp* transcripts (~2-fold) in B cells (Fig. 1*C*). *Ganp*^{Tg} mice had normal B lineage differentiation by surface marker studies of B220, IgM, and IgD on lymphoid cells in the bone marrow, spleen, and lymph nodes (Fig. 1*D*). B cell numbers and the levels of serum Igs were also normal in *Ganp*^{Tg} mice (data not shown). These results demonstrated that B cell differentiation undergoes normally in *Ganp*^{Tg} mice compared with wild-type littermates.

In vitro B cell proliferation and GC formation of Ganp^{Tg} *mice*

Next, we examined the potential of B cell proliferation of *Ganp*^{Tg} mice in vitro. *Ganp*^{Tg} mice showed comparable proliferation activities to wild-type littermates in response to anti-μ Ab, anti-μ Ab plus anti-CD40 mAb, or LPS (Fig. 1*E*). Interestingly, *Ganp*^{Tg} B cells showed augmented responses to anti-CD40 stimulation in comparison to wild-type B cells. This was only observed in the response to anti-CD40 stimulation but not in the response to anti-μ Ab or LPS stimulation, suggesting that *Ganp*^{Tg} mice augment CD40-stimulated response in vivo.

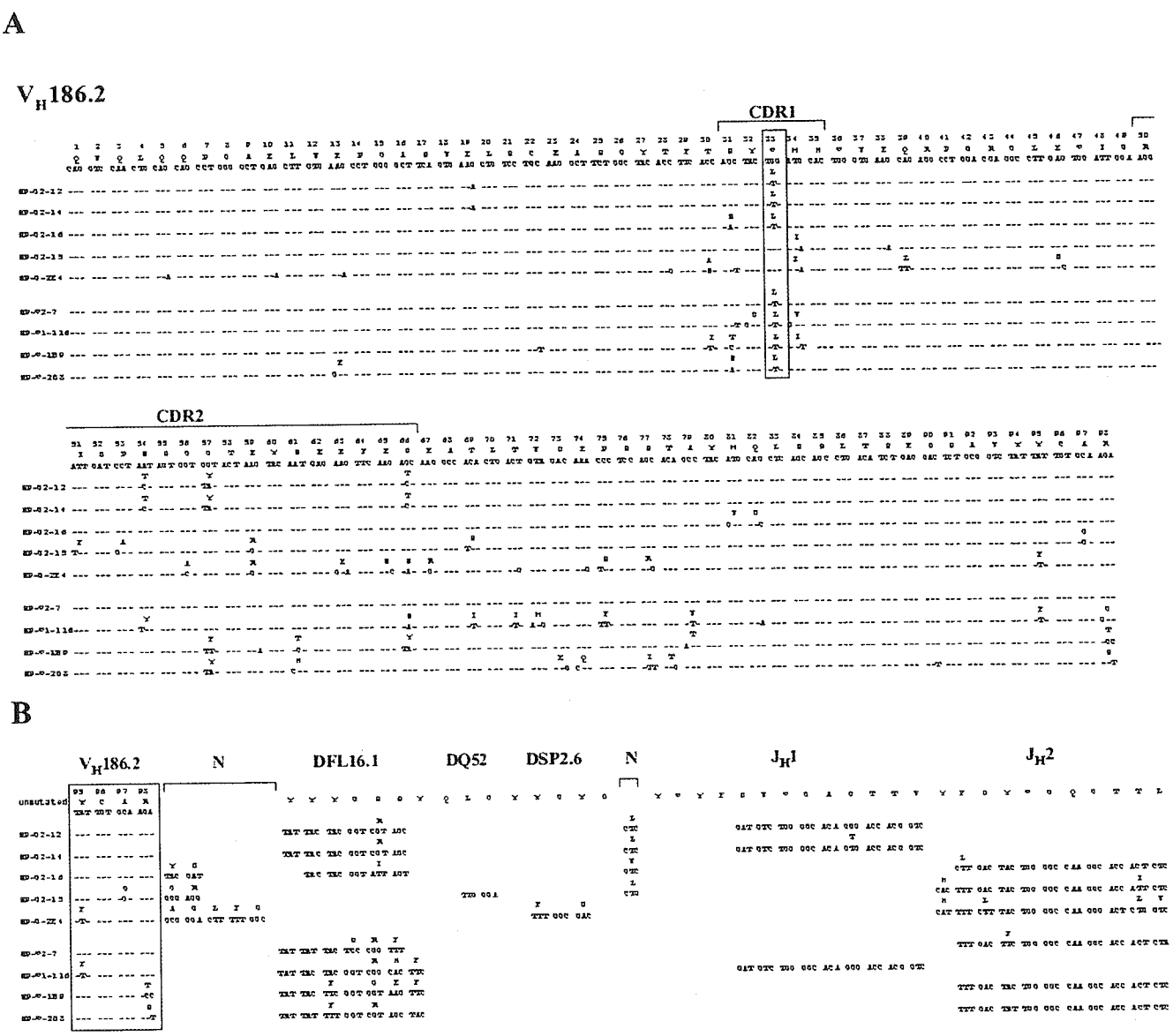

FIGURE 2. *(continues)*

We examined whether *Ganp*^{Tg} mice showed the alteration of GC formation in vivo. *Ganp*^{Tg} mice did not show any difference in the size and number of GCs at day 10 after SRBC immunization; however, in contrast to the findings observed in B-*ganp*$^{-/-}$ mice (4), *Ganp*^{Tg} mice showed the accelerated resolution of GC formation in vivo (Fig. 1*F*). This response could be due to the efficient production of high-affinity Ab in *Ganp*^{Tg} mice.

Responses of Ganp^{Tg} *mice against T cell-independent Ag and TD-Ag*

Because GANP expression is selectively up-regulated in GC B cells, we studied the Ab responses of *Ganp*^{Tg} mice. After Ag immunization, the responses were measured for T cell-independent type II Ag and TD-Ag at various time points and the results of day 14 were shown. The serum titers of Ag-specific Abs against TNP-Ficoll as T cell-independent Ag and TNP-KLH as TD-Ag were normal with similar distributions of various Ig isotypes in comparison with wild-type littermates (Fig. 1*G*).

Enhanced affinity maturation of Ganp^{Tg} *mice against TD-Ag*

However, after immunization with NP-CG, *Ganp*^{Tg} showed high affinity by the differential ELISA with the pauci NP_2-BSA conjugate that yielded 42% of the response to the multihapten NP_{17}-BSA conjugate in comparison with C57BL/6 (Fig. 1*H*). Jacob et al. (15, 16) showed that, in (NP-CG)-immunized C57BL/6 mice, the Abs in the secondary response against NP were exclusively IgG1/λ1 and had a single V_H region (V_H186.2) carrying with a peculiar pattern of mutation for high affinity. We investigated whether the affinity increase of anti-NP Ab generated in *Ganp*^{Tg} mice accompanied with the similar mutation pattern in the *V_H186.2* locus. The *V_H186.2* sequence was studied by RT-PCR using the spleen B cells from (NP-CG)-immunized mice. *Ganp*^{Tg} showed striking increases in mutation at ^{33}W to L of the *V_H186.2* locus in splenic B cells (W33L; Fig. 1*I*). These results demonstrated that *Ganp*^{Tg} induced a higher frequency of the high-affinity mutation during the immune response to TD-Ag.

Establishment of hybridomas secreting high-affinity anti-NP-hapten

Anti-NP hybridomas were established by immunization of *Ganp*^{Tg} with NP-CG. Supernatants from >6000 clones were screened by the differential ELISA to identify wells with high-affinity mAbs, and the selected hybridoma cells were cloned. Affinities of those

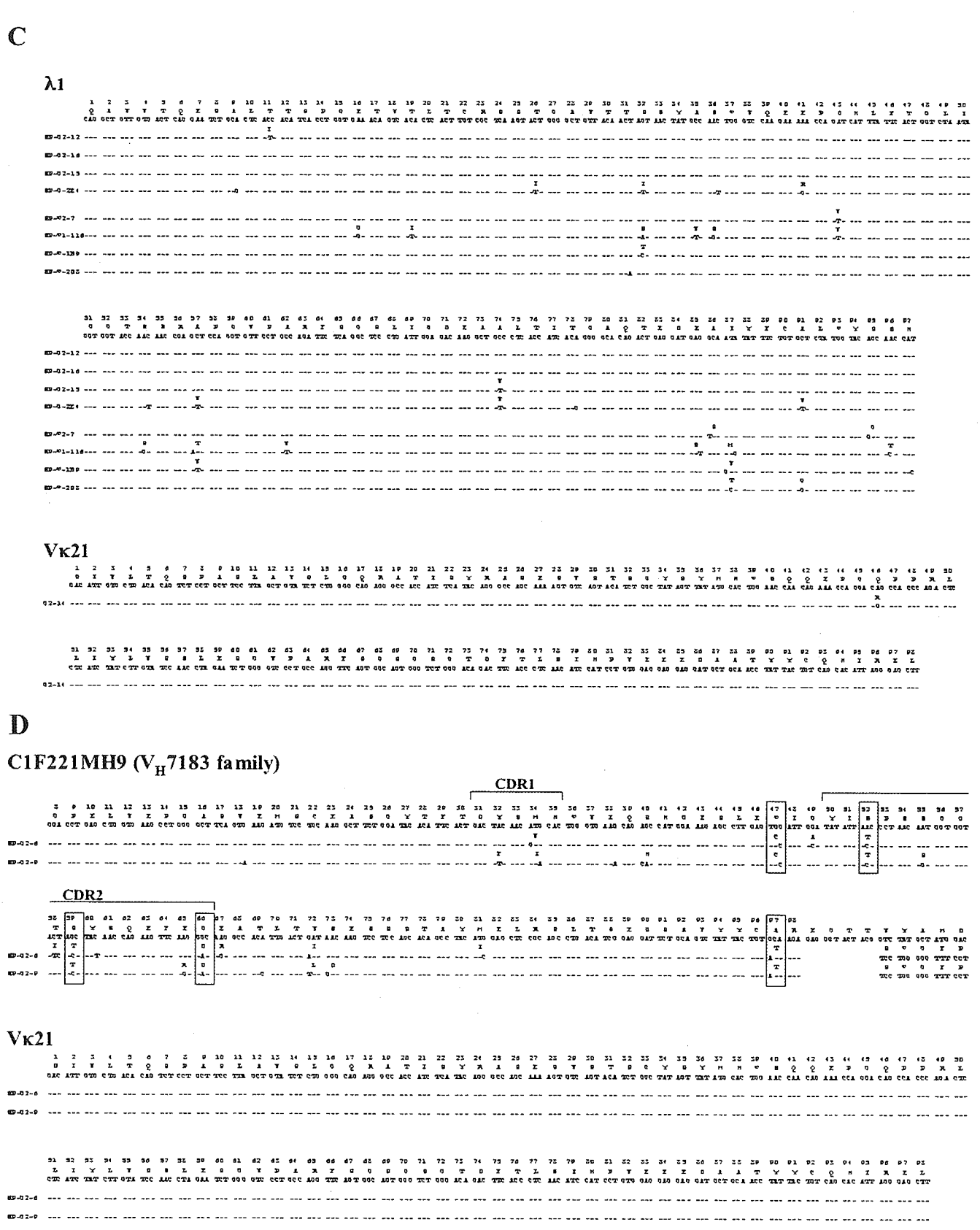

FIGURE 2. Sequence analysis of the *V* region genes of the hybridomas secreting anti-NP mAbs. V_H regions were determined using the primers commonly applicable to the major V_H families and the J_H4 primer (12). The individual *V* region sequence was determined after cloning of the genomic PCR products. Each sequence was determined by three sequencing reactions. *A*, The sequences of the clones using the V_H186.2 region are aligned and the site of W33L mutation is boxed. *B*, The sequences of the VDJ recombination regions are aligned. The part of the V_H186.2 region was boxed. *C*, The V_L region sequences were determined similarly to the method used for V_H regions. *D*, The sequences of the V_H and V_L regions of the two anti-NP mAbs that used noncanonical V_H regions are shown. The mutations shared between the two mAbs are boxed.

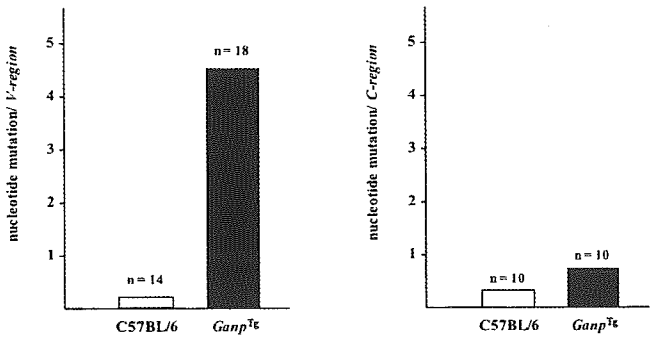

FIGURE 3. Mutation frequency induced in the V_H7183 family gene (C1F221MH9) by NP-CG immunization. NP-binding GC B cells were purified by a cell sorter 14 days after immunization with NP-CG in $Ganp^{Tg}$ and C57BL/6 mice. The V_H7183 family gene and $C\mu$ gene were PCR-amplified by Pfu-Turbo with genomic DNAs, cloned into TOPO cloning vector, and then sequenced. The mutation frequencies were counted based on the genomic sequences in the European Molecular Biology Laboratory database and were shown as average mutations per V_H region or $C\mu$ region sequences. The number (n) shows the V_H region (*left*) or $C\mu$ region (*right*) DNAs cloned in the TOPO cloning vector.

mAbs, after purification from clone culture supernatants, to NP-hapten were measured by the BIAcore system with a sensor chip conjugated with NP using Pharmacia Kinetics Evaluation software (9). The K_D of each mAb was determined by measuring the rate of binding to the Ag at different protein concentrations. The affinity of mAbs from (NP-CG)-immunized $Ganp^{Tg}$ and C57BL/6 mice were compared and the representatives were shown (Table I). The high-affinity mAbs of C57BL/6 mice used the $V_H186.2$ region in combination with λ1 L chain and yielded affinities from $K_D = 1.51 \times 10^{-7}$ M to 1.0×10^{-8} M. The mAbs from $Ganp^{Tg}$ showed the usage of canonical V_H186.2 in combination with both κ and λ yielding affinities from $K_D = 1.10 \times 10^{-7}$ M to 1.57×10^{-9} M. Interestingly, the mAbs from $Ganp^{Tg}$ also used noncanonical V_H region of V_H7183 family in combination κ-chain but showed similarly high affinities.

The usage and mutation of V *region genes in the anti-NP hybridomas*

The high-affinity mAbs obtained from C57BL/6 mice used the canonical $V_H186.2$ gene with the W33L mutation that is responsible for high affinity. This change increased the affinity from $K_D = 2 \sim 4 \times 10^{-6}$ M to 2×10^{-7} M (17, 18). The other mutations in the $V_H186.2$ gene segment would not have contributed to increased affinity against NP-hapten (19). Therefore, we sequenced the V_H regions of the hybridomas to examine whether there were similar mutation profiles of the V region. The mAbs from C57BL/6 mice generated typical high affinity against NP-hapten by using the $V_H186.2$ region with W33L mutation in combination with $DFL16.1$ and J_H2 gene segments. $Ganp^{Tg}$ generated similar high-affinity mAbs (NP-G2-12; $K_D = 4.92 \times 10^{-8}$, NP-G2-16; 1.10×10^{-7} M) (Table I) with the V_H186.2 having the W33L mutation (Fig. 2*A*). Interestingly, two anti-NP hybridomas that did not bear the W33L mutation in V_H186.2 showed similar high affinities. NP-G2-15 had the mutation of Y99G as reported previously (10). NP-G-2E4 with higher affinity ($K_D = 1.57 \times 10^{-9}$ M) did not have either of these two mutations but instead showed 13 aa mutations (22 nt changes) in the V_H186.2 region with the usage of DSP2.6 and J_H2 regions (Fig. 2, *A* and *B*). The L chain of NP-G-2E4 also had 6 aa mutations (10 nt changes) (Fig. 2*C*). This result suggested that the high affinity of NP-G-2E4 was generated by the extraordinarily increased V region mutations.

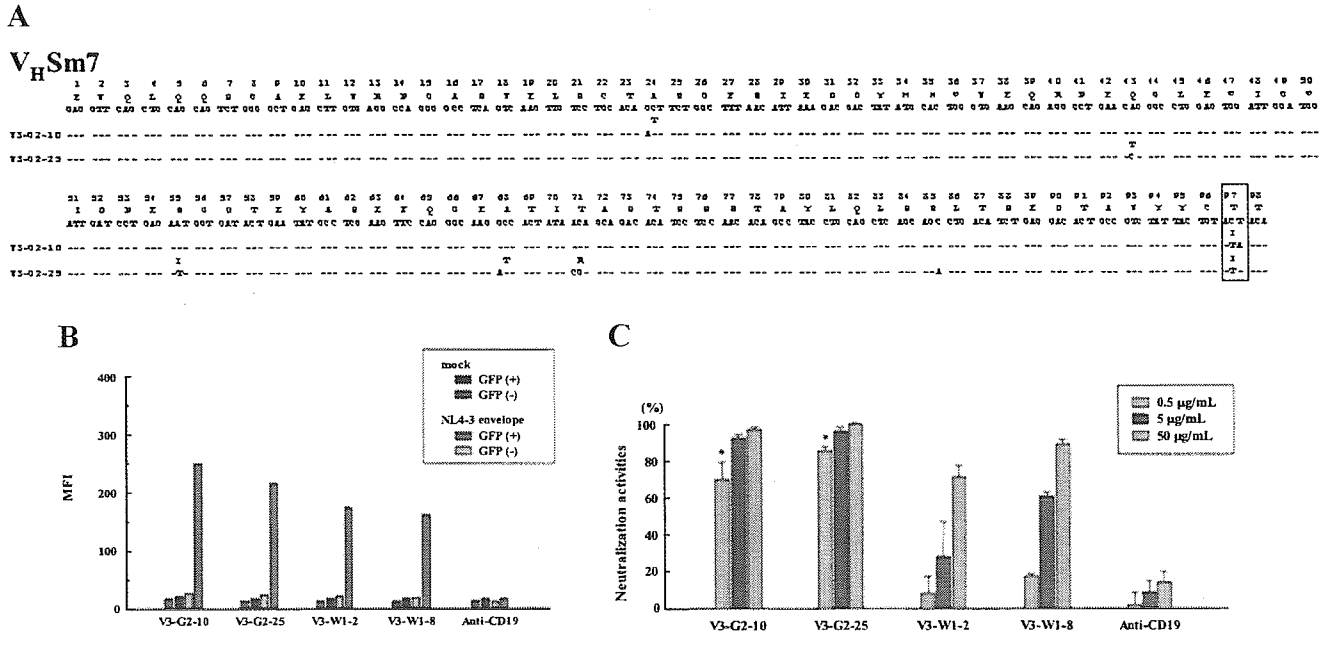

FIGURE 4. The sequences of the V_H region, the Ag-binding activities, and the neutralizing activities of the mAbs against the V3 epitope of HIV-1 gp120. *A*, The V_H region sequence (V_HSm7) used for the high-affinity mAbs from $Ganp^{Tg}$ is shown. The mutation site commonly observed in the two V_H sequences is boxed. *B*, Binding activity of the mAbs against HIV-1 envelope. Specific binding of the mAbs were shown as mean fluorescence intensity (MFI) examined with allophycocyanin-conjugated goat anti-mouse IgG Ab in combination with the NL4-3 envelope-expressing GFP^+-transfectants by using flow cytometry. Negative controls were measured with GFP^--mock transfectants. Another negative control for mAb binding was shown by CD19 mAb. *C*, Neutralizing activities were measured using a CD4-LTR/β-galactosidase-induced HeLa cell line. After $TCID_{50}$ of virus stock was predetermined with MAGI/CCR5 cells, the virus infection assay was conducted in vitro, to which anti-V3 epitope mAbs were added. Higher neutralization activities were significant (*) for the mAbs produced by $Ganp^{Tg}$ (V3-G2-10 and V3-G2-25) as compared with those of C57BL/6 mice at the concentration of 0.5 μg/ml. Negative control is shown with anti-CD19.

Moreover, two anti-NP mAbs from *Ganp*^{Tg} yielding similarly high affinities (K_D = 3.24 ~ 7.05 × 10^{-8} M) used noncanonical V_H region sequences, both of which probably originated from the same genomic *V_H7183* family. The best match in the Celera Discovery System was to the C1F221MH9 (*V_H7183* family), but the two clones showed variations with >12 nt differences from the genomic C1F221MH9 sequence (Fig. 2*D*). Mutations of W47C, N52C, S59T, G66D, and A97T were commonly observed in the V_H region (C1F221MH9), suggesting their contributions to raise the affinity of the mAb against NP-hapten. However, mutations in the V_L regions were not apparently increased in the comparison of the anti-NP mAbs from *Ganp*^{Tg} and C57BL/6 mice. The generation of high-affinity BCR without the exchange at position 33 is a rare event, which suggested that the combination of particular D-J_H sequences and/or many SHMs do not result in high affinity (18). A recent report only showed the case of mutation, Y99G in V_H186.2, which generated similar high-affinity mAb against NP-hapten comparable to W33L (10). Extensive earlier studies of anti-NP mAbs found that repeated immunization of C57BL/6 mice with NP-CG increased usage of noncanonical V_H regions and different L chain combinations (16). However, as far as we know, no study with conventional animals has demonstrated comparable high-affinity mAbs to those reported in this study. Although crystallographic studies are needed for definitive conclusions, we speculate that hypermutated C1F221MH9 V_H region (V_H7183 family) in association with other L chain combinations creates an effective tertiary structure for Ag-binding, yielding closer interactions of hypermutated C1F221MH9 V_H region and NP-hapten, and might be as effective as mAbs with the V_H186.2 region.

Mutations induced in the noncanonical V_H region of the spleen B cells after immunization with NP-CG

Usually wild-type C57BL/6 mice do not induce such a frequent mutation in the noncanonical V_H region in GC B cells before and after immunization with NP-CG. We examined the mutation frequency of the *V_H7183* family gene (C1F221MH9) under a non-immunization condition in spleen B cells of *Ganp*^{Tg} mice but found no alteration of the *V_H* region (data not shown). To study whether such hypermutation could be observed in *Ganp*^{Tg} spleen B cells after immunization, we investigated mutations in the *V_H7183* family gene (C1F221MH9) by examining genomic DNA of NP-binding GC B cells purified by cell sorting. These DNAs showed 16-fold higher mutation frequencies (4.5 mutations/*V_H* region of *Ganp*^{Tg} mAb vs 0.28 mutations/*V_H* region of C57BL/6 mAb) in the *V_H7183* family (Fig. 3, *left panel*). In contrast, such higher mutation frequencies were not observed in the Cμ region (Fig. 3, *right panel*). This is in agreement with the suggestion that *Ganp*^{Tg} has a high frequency of SHM that contributes to the production of high-affinity BCR in vivo. Alternatively, *Ganp*^{Tg} might effectively rescue and maintain B cells with high-affinity BCR during the immune response.

Establishment of high-affinity mAbs against HIV-1 by use of Ganp^{Tg} *mice*

To apply this system for generating high-affinity Ab using *Ganp*^{Tg} mice, we studied whether high-affinity anti-HIV-1 mAbs with significant neutralization activity against virus infection could be generated by immunization with the V3 loop peptide (NL4-3) of HIV-1 gp120. Differential ELISA using plates coated with high and low doses of the V3 peptide initially identified hybridoma cells with relatively high-affinity mAbs from >6000 wells of (V3 peptide)-immunized *Ganp*^{Tg} and C57BL/6 mice. High-affinity clones were selected from each mouse strain. After further cloning, individual mAbs were purified and their affinities were measured using the BIAcore system. The mAbs from both mouse systems showed higher affinities in a range from K_D = 2.81 × 10^{-5} M to ~ 5.67 × 10^{-9} M. However, we could obtain extraordinarily higher affinity mAbs (V3-G2-10 and V3-G2-25; K_D = 9.90 × 10^{-11} M) from *Ganp*^{Tg} over the level that is generally not attainable by conventional methods of mAb preparation (20). The highest affinity mAbs (V3-W1-2 and V3-W1-8) from C57BL/6 mice were up to K_D = 9.81 × 10^{-8} M and 7.58 × 10^{-8} M. The high-affinity mAbs from *Ganp*^{Tg} used the same V_H region (V_HSm7) with the common mutation at T97I, suggesting that the T97I mutation contributed to an affinity increase against the V3 epitope (Fig. 4*A*). A binding assay involving HIV-1 envelope (NL4-3) gene-transfected cells was used to determine whether the mAb recognized the viral epitope. The binding activities to the transfectants were studied by flow cytometry as mean fluorescence intensity in comparison with the GFP-positivity as indicators of gene transfection. The mAbs (V3-G2-10, V3-G2-25, V3-W1-2, and V3-W1-8) showed higher binding activities to the virus epitope-expressing cells (Fig. 4*B*).

The neutralization activities of these anti-HIV-1 mAbs were examined using a CD4-LTR/β-galactosidase-transduced HeLa cell line that expresses high levels of human CD4 and contains a single integrated copy of a *β-galactosidase* gene under the control of a truncated HIV-1 LTR (13, 21). Neutralization activities of the two high-affinity mAbs (V3-G2-10 and V3-G2-25) were clearly detected at 0.5 μg/ml, which were more effective than those of mAbs (V3-W1-2 and V3-W1-8) from C57BL/6 (Fig. 4*C*). The simple comparison might indicate 50–100 times increase of affinity in the mAbs from *Ganp*^{Tg} mice. These mAbs with high-affinity Ag-binding and neutralization activities should be useful for clinical diagnostic purposes and analogous human mAbs might have therapeutic possibilities (22).

Discussion

Expression of GANP is required for generation of high-affinity Ab response in vivo, which was demonstrated by conditional targeting of *ganp* gene in B cells that caused apparent decrease in production of high-affinity Ab against NP-hapten, accompanied with the decreased frequency of high-affinity type mutation of W33L at the V_H186.2 in NP-binding IgG1$^+$ B cells (5). Several possibilities might be considered to explain the mechanism of GANP in generation of high-affinity BCR$^+$ B cells in vivo. GANP might be directly linked in genetic alteration, including *V* region dsDNA breaks occurring in B cell proliferation (23), SHM events in association with activation-induced cytidine deaminase (24), uracil DNA glycosylase (25), and error-prone DNA polymerases up-regulated in GC B cells (26), DNA recombination and repair mechanisms or rather involved in the selection of high-affinity BCR$^+$ B cells in the follicular dendritic cell network (27), and survival and maintenance of B cells with high-affinity type mutations throughout the immune response.

There are several possible mechanisms regarding the GANP function. Firstly, GANP might directly regulate generation of mutation frequency of the V_H region in GC B cells. The structure and expression of GANP indicated that GANP has two nuclear localization signal sequences (^{497}HKKK and ^{1344}PMKQKRR), two putative nuclear export signal sequences, and appears mostly in the nucleus but is also in the cytoplasm (our unpublished observation). The C-terminal region is capable of binding and acetylating with MCM3 of the MCM-complex that bears DNA helicase activity and is essential for DNA replication (28). In the N-terminal side, there is a putative RNA-associated region as the RNA recognition motif. The RNA-primase region and the RNA-binding activity might cooperate during the transcription at G_1 phase and introduce the alteration or the damage of the *V_H* region sequences during rapid cell proliferation in GCs. More interestingly, altered expression of

mouse SHD1 that has a homology to the central part of GANP (630–950 aa) caused an apparent cell cycle abnormality involving with centrosome duplication and M phase transition (29), which was also in accordance with the information of the association of *Saccharomyces* Sac3 with Cdc31/centrin (30). Loss of SHD1 caused an impairment of centrosome duplication, deregulated nuclear division, with disappearance of Mad2 expression in the prometaphase. Because mouse GANP is considered as a homologue of *Saccharomyces* Sac3 (31), GANP might be also involved in the centrosome duplication or the chromatin segregation during cell division. These observations suggested the involvement of GANP in either one or several mechanisms of gene transcription, DNA replication, and chromatin separation and cell division. Loss of GANP caused the increased apoptotic cells in GCs after immunization with TD-Ags (4), whereas the gain of function did not show obvious difference (data not shown). Second, these functions of GANP regions might be involved in the repair of DNA injuries occurring under a transcription-coupled mechanism or in the DNA replication phase. If this is the case, existence of GANP is critical for maintenance of DNA stability during the GC B cell stage that undergoes genetic alteration with frequent SHM of the V_H region and class switch recombination. Expression of GANP is necessary for the rescue of damaged GC B cells that potentially gain the high-affinity BCR. Third, additional function of GANP might be involved in generation or selection of high-affinity BCR^+ B cells in GCs. $Ganp^{Tg}$ mice showed accelerated kinetics of GC formation (Fig. 1*F*), whereas B-$ganp^{-/-}$ mice showed retarded GC formation (4). Recently, Mirnics et al. (32) described that GANP is involved in downstream event(s) of Lyn. As Lyn is involved in CD40-mediated signal transduction (33) and Lyn-deficient mice showed lack of GCs (34), there might be functional interaction of CD40-mediated signaling with the GANP function involved in regulation of high-affinity B cells. The augmented anti-CD40 response of $Ganp^{Tg}$ mice might support this notion, in which GANP is necessary for the rescue of high-affinity B cells during the selection in GCs. As a potential role of GANP in the selection process, GANP associates with a protein phosphatase component G5PR that associates with protein phosphatase 5 and protein phosphatase 2A (35). The complex of GANP with G5PR may regulate the other signaling pathways involved in cell survival mechanism or in regulation of BCR-mediated cell proliferation during maturation and selection of GC B cells. We have no definitive evidence to conclude the molecular mechanism at present but GANP is most likely a key molecule to elucidate the molecular mechanism in generation of high-affinity Ab in vivo.

To confirm the effect of GANP in generation of high-affinity Ab, we used a system to compare the affinity of the Abs at the monoclonal level by establishing the mAb-producing hybridomas. Affinity measurement with NP-hapten clearly demonstrated the high affinity of the mAbs generated from the $Ganp^{Tg}$ mice. Sequence analyses of the *V* regions of individual mAb-producing hybridomas demonstrated that the high affinity was generated not only with increased SHM frequency in the $V_H186.2$ region but also with the noncanonical V_H region usage that was not seen in the control hybridomas.

The results of both the loss and gain of GANP expression caused adverse effects in generation of high affinity response, which confirmed that the GANP function is involved in generation of high-affinity Ab in vivo. Additionally, the high-affinity is generated with the genetic alteration of *V* region genes as increased SHM and the different *V* region usage. GANP function might be directly involved in the formation of high affinity V region of the GC B cells. GANP is not up-regulated in the nonimmunized condition and is not expressed in normal T cells at the similar level detected with anti-GANP mAb (3). We speculate that up-regulation of GANP is selective in the cells with frequent genetic alterations such as *V* region SHM and class switch recombination during rapid proliferation phase.

In summary, we have demonstrated that $Ganp^{Tg}$ induces higher affinity Ab against TD-Ag in vivo, which was confirmed by BIAcore system with the purified mAbs against two model Ags of NP-hapten and the gp120 V3 peptide of HIV-1 by immunizing as TD-Ag. More importantly, the usage and the mutations of the V regions demonstrated that increased expression of GANP caused the genetic alteration of the *V* regions with increased mutations generating high affinity against TD-Ag in vivo. The results suggest that the $Ganp^{Tg}$ mouse has an advantage in preparation of mAbs against various epitopes, for which conventional mice hardly generate high-affinity mAbs by the standard procedures. High-affinity mAbs generated this way show greater epitope binding constants and this binding is long-lasting as measured in vitro. It would be useful to generate high-affinity mAbs against various molecules, which can be applicable widely in the diagnostic and therapeutic purposes.

Acknowledgments

We appreciate Dr. Y. Takahashi and Dr. T. Takemori for helpful advice and Y. Kumamoto for technical assistance.

Disclosures

The authors have no financial conflict of interest.

References

1. MacLennan, I. C. M. 1994. Germinal centers. *Annu. Rev. Immunol. 12:117.*
2. Rajewsky, K. 1996. Clonal selection and learning in the antibody system. *Nature 381:751.*
3. Kuwahara, K., M. Yoshida, E. Kondo, A. Sakata, Y. Watanabe, E. Abe, Y. Kouno, S. Tomiyasu, S. Fujimura, T. Tokuhisa, et al. 2000. A novel nuclear phosphoprotein, GANP, is up-regulated in centrocytes of the germinal center and associated with MCM3, a protein essential for DNA replication. *Blood 95:2321.*
4. Kuwahara, K., S. Tomiyasu, S. Fujimura, K. Nomura, Y. Xing, N. Nishiyama, M. Ogawa, S. Imajoh-Ohmi, S. Izuta, and N. Sakaguchi. 2001. Germinal center-associated nuclear protein (GANP) has a phosphorylation-dependent DNA-primase activity that is up-regulated in germinal center regions. *Proc. Natl. Acad. Sci. USA 98:10279.*
5. Kuwahara, K., S. Fujimura, Y. Takahashi, N. Nakagata, T. Takemori, S. Aizawa, and N. Sakaguchi. 2004. Germinal center-associated nuclear protein contributes to affinity maturation of B cell antigen receptor in T cell-dependent responses. *Proc. Natl. Acad. Sci. USA 101:1010.*
6. Koike, M., Y. Kikuchi, A. Tominaga, S. Takaki, K. Akagi, J. Miyazaki, K. Yamamura, and K. Takatsu. 1995. Defective IL-5-receptor-mediated signaling in B cells of X-linked immunodeficient mice. *Int. Immunol. 7:21.*
7. Jonsson, U., L. Fagerstam, B. Ivarsson, B. Johnsson, R. Karlsson, K. Lundh, S. Lofas, B. Persson, H. Roos, I. Ronnberg, et al. 1991. Real-time biospecific interaction analysis using surface plasmon resonance and a sensor chip technology. *BioTechniques 11:620.*
8. Johnsson, B., S. Lofas, and G. Lindquist. 1991. Immobilization of proteins to a carboxymethyldextran-modified gold surface for biospecific interaction analysis in surface plasmon resonance sensors. *Anal. Biochem. 198:268.*
9. Karlsson, R., A. Michaelsson, and L. Mattsson. 1991. Kinetic analysis of monoclonal antibody-antigen interactions with a new biosensor based analytical system. *J. Immunol. Methods 145:229.*
10. Furukawa, K., A. Akasako-Furukawa, H. Shirai, H. Nakamura, and T. Azuma. 1999. Junctional amino acids determine the maturation pathway of an antibody. *Immunity 11:329.*
11. Chen, J., P. Borden, J. Liao, and E. A. Kabat. 1992. Variable region cDNA sequences of three mouse monoclonal anti-idiotypic antibodies specific for anti-$\alpha_{1\rightarrow6}$ dextrans with groove- or cavity-type combining sites. *Mol. Immunol. 29:1121.*
12. Wei, C., R. Zeff, and I. Goldschneider. 2000. Murine pro-B cells require IL-7 and its receptor complex to up-regulate IL-7Rα, terminal deoxynucleotidyltransferase, and cμ expression. *J. Immunol. 164:1961.*
13. Kimura, T., K. Yoshimura, K. Nishihara, Y. Maeda, S. Matsumi, A. Koito, and S. Matsushita. 2002. Reconstitution of spontaneous neutralizing antibody response against autologous human immunodeficiency virus during highly active antiretroviral therapy. *J. Infect. Dis. 185:53.*
14. Reed, L. J., and H. Muench. 1938. A simple method of estimating fifty percent end points. *Am. J. Hyg. 27:493.*
15. Jacob, J., G. Kelsoe, K. Rajewsky, and U. Weiss. 1991. Intraclonal generation of antibody mutants in germinal centres. *Nature 354:389.*
16. Jacob, J., J. Przylepa, C. Miller, and G. Kelsoe. 1993. In situ studies of the primary immune response to (4-hydroxy-3-nitrophenyl)acetyl. III. The kinetics of

V region mutation and selection in germinal center B cells. *J. Exp. Med. 178:1293.*
17. Cumano, A., and K. Rajewsky. 1986. Clonal recruitment and somatic mutation in the generation of immunological memory to the hapten NP. *EMBO J. 5:2459.*
18. Allen, D., T. Simon, F. Sablitzky, K. Rajewsky, and A. Cumano. 1988. Antibody engineering for the analysis of affinity maturation of an anti-hapten response. *EMBO J. 7:1995.*
19. French, D. L., R. Laskov, and M. D. Scharff. 1998. The role of somatic hypermutation in the generation of antibody diversity. *Science 244:1152.*
20. Poignard, P., T. Fouts, D. Naniche, J. P. Moore, and Q. J. Sattentau. 1996. Neutralizing antibodies to human immunodeficiency virus type-1 gp120 induce envelope glycoprotein subunit dissociation. *J. Exp. Med. 183:473.*
21. Kimpton, J., and M. Emerman. 1992. Detection of replication-competent and pseudotyped human immunodeficiency virus with a sensitive cell line on the basis of activation of an integrated β-galactosidase gene. *J. Virol. 66:2232.*
22. Matsushita, S., H. Maeda, K. Kimachi, Y. Eda, Y. Maeda, T. Murakami, S. Tokiyoshi, and K. Takatsuki. 1992. Characterization of a mouse/human chimeric monoclonal antibody (Cβ1) to a principal neutralizing domain of the human immunodeficiency virus type 1 envelope protein. *AIDS Res. Hum. Retroviruses 8:1107.*
23. Wu, X., J. Feng, A. Komori, E. C. Kim, H. Zan, and P. Casali. 2003. Immunoglobulin somatic hypermutation: double-strand DNA breaks, AID and error-prone DNA repair. *J. Clin. Immunol. 23:235.*
24. Honjo, T., K. Kinoshita, and M. Muramatsu. 2002. Molecular mechanism of class switch recombination: linkage with somatic hypermutation. *Annu. Rev. Immunol. 20:165.*
25. Storb, U., and J. Stavnezer. 2002. Immunoglobulin genes: generating diversity with AID and UNG. *Curr. Biol. 12:R725.*
26. Jacobs, H., and L. Bross. 2001. Towards an understanding of somatic hypermutation. *Curr. Opin. Immunol. 13:208.*
27. van Eijk, M., T. Defrance, A. Hennino, and C. de Groot. 2001. Death-receptor contribution to the germinal-center reaction. *Trends Immunol. 22:677.*
28. Bailis, J. M., and S. L. Forsburg. 2004. MCM proteins: DNA damage, mutagenesis and repair. *Curr. Opin. Genet. Dev. 14:17.*
29. Khuda, S. E., M. Yoshida, Y. Xing, T. Shimasaki, M. Takeya, K. Kuwahara, and N. Sakaguchi. 2004. The *Sac3* homologue *shd1* is involved in mitotic progression in mammalian cells. *J. Biol. Chem. 279:46182.*
30. Fischer, T., S. Rodriguez-Navarro, G. Pereira, A. Racz, E. Schiebel, and E. Hurt. 2004. Yeast centrin Cdc31 is linked to the nuclear mRNA export machinery. *Nat. Cell Biol. 6:840.*
31. Bauer, A., and R. Kölling. 1996. Characterization of the SAC3 gene of *Saccharomyces cerevisiae. Yeast 12:965.*
32. Mirnics, Z. K., E. Caudell, Y. Gao, K. Kuwahara, N. Sakaguchi, T. Kurosaki, J. Burnside, K. Mirnics, and S. J. Corey. 2004. Microarray analysis of Lyn-deficient B cells reveals germinal center-associated nuclear protein and other genes associated with the lymphoid germinal center. *J. Immunol. 172:4133.*
33. Ren, C. L., T. Morio, S. M. Fu, and R. S. Geha. 1994. Signal transduction via CD40 involves activation of *lyn* kinase and phosphatidylinositol-3-kinase, and phosphorylation of phospholipase Cγ2. *J. Exp. Med. 179:673.*
34. Nishizumi, H., I. Taniuchi, Y. Yamanashi, D. Kitamura, D. Ilic, S. Mori, T. Watanabe, and T. Yamamoto. 1995. Impaired proliferation of peripheral B cells and indication of autoimmune disease in *lyn*-deficient mice. *Immunity 3:549.*
35. Kono, Y., K. Maeda, K. Kuwahara, H. Yamamoto, E. Miyamoto, K. Yonezawa, K. Takagi, and N. Sakaguchi. 2002. MCM3-binding GANP DNA-primase is associated with a novel phosphatase component G5PR. *Genes Cells 7:821.*

J Med Dent Sci 2003; 50: 17–25

Original Article

TNF-related apoptosis-inducing ligand (TRAIL) induces neuronal apoptosis in HIV-encephalopathy

Yoshiharu Miura[1], Yoshio Koyanagi[2] and Hidehiro Mizusawa[1]

1) Department of Neurology and Neurological Science (Chairman: Prof. Hidehiro Mizusawa), Graduate School, Tokyo Medical and Dental University
2) Department of Virology, Tohoku University Graduate School of Medicine, Sendai

Neuronal loss is frequently found in brains of patients with human immunodeficiency virus (HIV)-encephalopathy. Extensive apoptosis of neurons is probably involved in the development of HIV-encephalopathy. The present study was designed to investigate the mechanism of neuronal apoptosis. For this purpose, we examined autopsy brains of two patients with HIV-encephalopathy. Terminal deoxynucleotidyl transferase-mediated dUTP nick-end labeling (TUNEL)-positive cells and active forms of caspase-3- and -8-positive cells, including neurons, were found in the perivascular regions of the brains. In these regions, TNF-related apoptosis-inducing ligand (TRAIL)$^+$ macrophages were also observed. We also examined brains of HIV-1-infected mouse model inoculated with human cells. In these brains, TUNEL$^+$ neurons were also found in the perivascular region, the site where infiltrated HIV-1-infected and TRAIL-expressing macrophages were observed. Using an *in vitro*-culture system, we also demonstrated that the HIV-1-infected monocyte-derived macrophages preferentially expressed TRAIL and that the addition of HIV-1-infected macrophages or human TRAIL-overexpressing mouse cells to cultured mouse primary neurons/glia resulted in neuronal apoptosis. Our results suggest the involvement of TRAIL expressed on HIV-1-infected macrophages in the induction of neuronal apoptosis in infected brain.

Key words: HIV-encephalopathy, TRAIL, neuronal apoptosis, caspase-8, HIV

Corresponding author: Yoshiharu Miura
Department of Neurology and Neurological Science, Graduate School, Tokyo Medical and Dental University
1-5-45, Yushima, Bunkyo-ku, Tokyo, Japan 113-8519
Phone: 81-3-5803-5234
Fax: 81-3-5803-0169
E-mail: ymiura@mail.cc.tohoku.ac.jp
Received November 15, 2002; Accepted January 14, 2003

Introduction

Human immunodeficiency virus (HIV)-encephalopathy is a cognitive/motor deficit complex in HIV-infected patients after long latent infection. The histopathological features of this encephalopathy include perivascular cuffing, microglial nodules, astrocytosis, neuronal degeneration, reduced synaptic density, myelin pallor, and occasional multinucleated giant cells[1]. In the infected brain, HIV infection has been confirmed only in monocyte/macrophage-lineage such as infiltrating macrophages and microglia, but not in neurons[2]. Although many factors induced by HIV-1 infection, such as viral proteins and host proteins, are thought to contribute to neuronal degeneration, the exact mechanism of this pathological process has not yet been identified[3]. Based on a series of histopathological analyses in autopsy brains, apoptosis of neurons was reported to play a major role in HIV-encephalopathy[4]. However, the pathways involved in this apoptotic process remain unknown at present.

TNF-related apoptosis-inducing ligand (TRAIL) is a new member of death-inducing ligands in the TNF family[5]. This death ligand activates caspase-8 and subse-

quently caspase-3 through its receptor and efficiently induces apoptotic cell death[6]. The human TRAIL molecule is capable of providing apoptosis signal to its murine receptors[7]. This property allows examination of the therapeutic application of human TRAIL *in vivo* using mouse tissues. While it has been reported that TRAIL induces apoptosis of various tumor cells[8], the pathological roles of TRAIL are largely unknown. In addition, recent studies reported that certain viral infections can augment TRAIL expression and induce TRAIL-mediated apoptosis[9,10]. Thus, it is possible that TRAIL is involved in HIV pathogenesis[11].

The present study was designed to examine the role of TRAIL expressed on HIV-infected macrophages in induction of neuronal apoptosis. Our results showed that apoptosis of neurons correlated with the presence of TRAIL-expressing macrophages in the brains of patients with HIV-encephalopathy and HIV-1-infected *in vivo*-murine model. Furthermore, the addition of HIV-1-infected macrophages or TRAIL-overexpressing mouse cells to cultured neurons/glia directly induced neuronal apoptosis. Our results suggest that TRAIL expressed on HIV-infected macrophages induces neuronal apoptosis in HIV-1-infected brain.

Materials and Methods

1. Brain specimens

Autopsy brains of two demented HIV-1-infected patients aged 48 and 25 years, who were free of opportunistic infection or tumor in the central nervous system (CNS), were kindly provided by Dr. K. Inoue (Faculty of Medicine, University of Tokyo). Postmortem tissues were fixed in 10% buffered formalin and embedded in paraffin. For negative control, non-demented HIV-1-uninfected brain was prepared. The study protocol was approved by the Human Ethics Review Committees of participating institutions.

2. Generation of human cell-transplanted mice and HIV-1 infection

Non-obese diabetic-severe combined immunodeficiency (NOD-SCID) mice were used at 6-8 weeks of age. The experimental protocol was approved by the Ethics Review Committee for Animal Experimentation of the participating institutions. The methods used for isolating human peripheral blood mononuclear cells (PBMC) and their infection with a green fluorescent protein (GFP)-expressing HIV-$1_{NL\text{-}CSFV3\text{-}EGFP}$ virus were described previously[11]. The GFP-expressing HIV-$1_{NL\text{-}CSFV3\text{-}EGFP}$ virus was constructed by replacing the V3 sequence in the HIV-$1_{NL\text{-}EGFP}$ with the V3 sequence from HIV-1_{JRCSF}[11,12]. Seven days later, the infected NOD-SCID mice were injected intraperitoneally with 100 μg of lipopolysaccharide (LPS) (Sigma, St. Louis, MO, USA). The mice were sacrificed 3 days later and the brains were dissected out, fixed in 4% periodate-lysine-paraformaldehyde (PLP) fixative, and then subjected to histopathological analyses. For negative control, brains of mice both inoculated with human PBMC and uninfected with HIV-1 were prepared.

3. Cell culture and staining

Cultures of mouse brain primary neurons/glia mixture were prepared from E 18 Balb/c mouse embryo as described previously[13]. Cells were maintained in high glucose-DMEM (Sigma) containing B27 components (Gibco, Tokyo). Seven days after initiation of culture, HIV-1-infected monocyte-derived macrophages (MDM) or human TRAIL- or Fas ligand (FasL)-expressing mouse B cells (hTRAIL/2PK-3 and hFasL/2PK-3, respectively)[14] were added and co-cultured for 4 days. The MDM had been enriched from PBMC of a HIV-1-seronegative healthy donor by plastic adherence and cultured in RPMI 1640 medium supplemented with 10% fetal calf serum and 5% giant cell tumor supernatant (IGEN, Rockville, MD, USA). MDM were infected with HIV-1_{JRFL} or HIV-$1_{NL\text{-}CSFV3\text{-}EGFP}$ at 7 days after plating. Co-cultured cells were fixed with 4% paraformaldehyde and stained with terminal deoxynucleotidyl transferase-mediated dUTP nick-end labeling (TUNEL) (Cy5, green), and anti-neurofilament protein (NFP) monoclonal antibody (mAb) (clone 2F11, Dako, Kyoto) immunochemically by means of EPOS (Dako) and TSA™-Direct method (NEN™ Life Science Products; NEN, Boston, MA, USA) as Cyanine 3 (red). NFP^+ $TUNEL^+$ apoptotic neurons were counted. Then, fixed MDM were incubated with anti-TRAIL antibody (Ab) (goat polyclonal IgG, Santa Cruz Biotechnology, Inc., Santa Cruz, CA, USA). Biotinylated donkey IgG against goat IgG (Polyscience Inc., Warrington, PA, USA) was used as secondary Ab, and followed by Alexa 568-conjugated streptavidin (Molecular Probes; FMP, Eugene, OR, USA).

4. Histopathological analyses

The fixed brain tissues were embedded in paraffin and cut into 6-μm thick sections. Sections were stained by hematoxylin and eosin (H&E), and immunohistochemically with the following Abs: anti-

HIVgag p24 mAb (clone Kal-1, Dako), anti-active form caspase-3 Ab (rabbit polyclonal IgG, R&D Systems, Minneapolis, MN, USA), anti-cleaved caspase-8 mAb (clone D384, mouse monoclonal IgG, Cell Signaling Technology, Beverly, MA, USA), or anti-TRAIL Ab (goat polyclonal IgG, Santa Cruz Biotechnology). For detection, the HISTOFINE indirect method (NICHIREI Co., Tokyo) or the TSA™-Indirect method (NEN) was performed as described previously[11]. Non-immunized immunoglobulin was used as a negative control.

TUNEL staining was carried out as described previously[11]. Absence of TdT served as a negative control. DNase-treated sections served as a positive control. Dual-color staining, including TUNEL, was performed with Alexa 568-conjugated streptavidin and FluoroNissl Green (FNG, FMP)[15]. Triple-color analysis for GFP, CD68, and TRAIL was performed with horseradish peroxidase-conjugated anti-human CD68 mAb (clone PGM1, Dako) and anti-TRAIL Ab (goat polyclonal IgG, Santa Cruz Biotechnology), followed by biotinylated donkey IgG against goat IgG (Polyscience Inc.), Cy5-conjugated streptavidin (Amersham Pharmacia Biotech, Tokyo), and Cyanine 3-conjugated tyramide (NEN). Negative controls were prepared without the use of the primary Ab. Sections were covered with a Vectorshield-mounting-medium and examined under a confocal laser-scanning microscope (model TCS NT, Leica, Mannheim, Germany). A single 488-nm beam for GFP and FNG, 542-nm for Cyanine 3 and Alexa 568, 600-nm for Cy5 from an argon-krypton laser were used for excitation. Emission from GFP or FNG was detected through a long-pass filter (< 540 nm) and was displayed as green color. Emission from Cyanine 3 or Alexa 568 was detected through a band-pass filter (600 ± 10 nm) and was displayed as red. Emission from Cy5 was detected through a band-pass filter (740 ± 70 nm) and was displayed as blue or green.

5. Statistical analysis

All data were expressed as mean ± SD. Differences between groups were examined for statistical significance using the Student's *t*-test. A P value less than 0.05 denoted the presence of a statistically significant difference.

Results

1. Histopathological analyses of the brains of HIV encephalopathy patients

We initially performed histopathological analyses of brains of two HIV-dementia patients. H&E staining indicated astrocytosis, macrophage infiltration, microglial nodules and multinucleated giant cells in the infected brains as described previously[1] (data not shown). HIV-1 p24$^+$ cells, which might produce HIV-1 virions, were macrophage and microglia but not neurons (Fig. 1e). These findings corresponded well with those of previous reports[1]. Importantly, we were able to

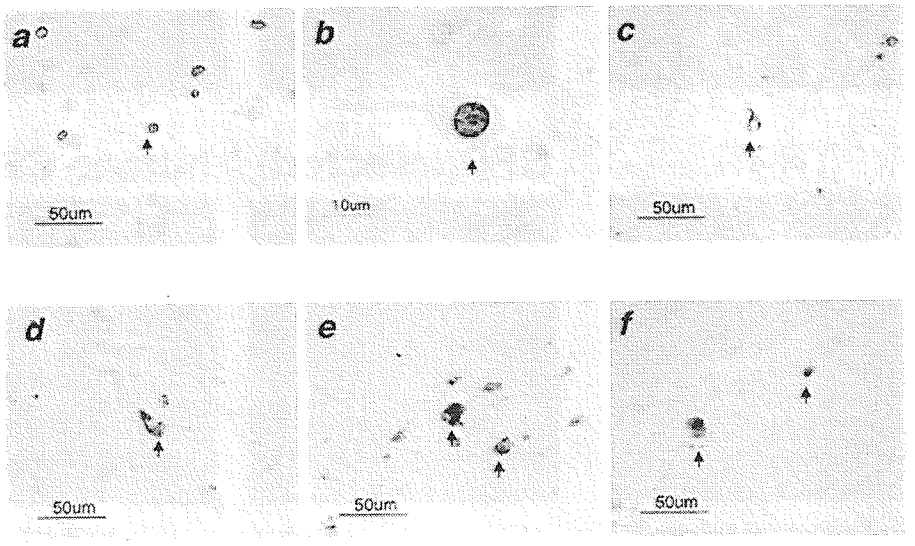

Fig. 1. Histopathological examination of brains of two patients with HIV-encephalopathy. TUNEL-positive (a, b), active form of caspase-3-positive (c), and cleaved caspase-8-positive (d) neurons are indicated by arrows. HIV p24-positive (e) and TRAIL-positive (f) cells are mainly macrophages (arrows). All marker-positive cells were found in the perivascular lesion of the frontal lobe.

find many TUNEL$^+$ apoptotic cells including neurons (more than 20 cells per slide) in the brains of these patients (Fig. 1a and b).

To identify the apoptosis-cascade, we immunostained brain sections using Abs against the active form of caspase-3 and cleaved caspase-8. A significant number of active form caspase-3- and cleaved caspase-8-positive cells including neurons were found in the perivascular regions of the frontal lobe (Fig. 1c and d). These data suggested that cells including neurons underwent apoptosis through caspase-3 and -8-pathways. Since upregulation of TRAIL expression has been reported in HIV-1 infected macrophages[16], and in both HIV-infected patients and hu-PBMC-SCID mice[11,17], TRAIL is a possible death ligand molecule in the HIV-1-infected brain. In fact, many macrophages, especially those infiltrating the perivascular region of the frontal lobe, preferentially expressed TRAIL in these patients (Fig. 1f).

2. Histopathological analyses of *in vivo* HIV-encephalopathy murine model

We also examined the brains of HIV-1-infected human PBMC-transplanted NOD-SCID mice after LPS inoculation. LPS is a potent activator of macrophage and can induce transmigration of these cells from the peripheral blood into CNS[18,19]. In these experiments, we used GFP-carrying HIV-1 which efficiently infect CD68$^+$ macrophages, and then human cells including GFP$^+$ HIV-1-infected macrophages to invade the brain. TUNEL$^+$ apoptotic neurons, which show Nissl body in the cytoplasm (a neuron-specific marker), and TRAIL$^+$ GFP$^+$ CD68$^+$ macrophages were frequently found in the perivascular region (Fig. 2). These results indicate that neuronal apoptosis is functionally associated with TRAIL expressing cells (i.e., virus-infected macrophages) in HIV-1-infected brain.

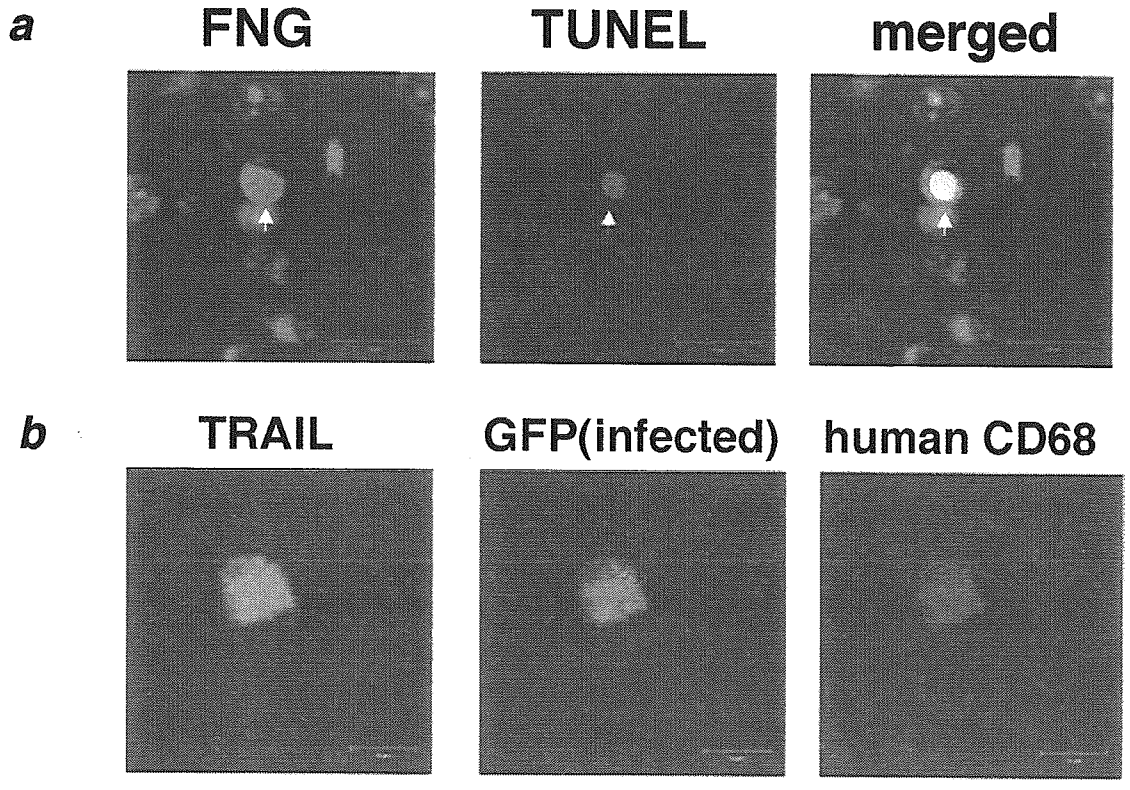

Fig. 2. Histopathological examination of brains of HIV-encephalopathy *in vivo*-murine model. Hu-PBMC-NOD-SCID mouse was infected with HIV and LPS was administered 7 days after infection. Three days later, the brain was dissected out and stained for histopathological examination. (a) Neuronal apoptosis was identified as nuclear TUNEL$^+$ and cytoplasmic FNG$^+$ cells, indicated by arrows, in the cerebral cortex of brain of HIV_{JRFL}-infected mouse. (b) TRAIL$^+$ GFP$^+$ human CD68$^+$ macrophages were found in the perivascular lesion of the cerebral cortex of GFP-carrying $HIV_{NL\text{-}CSFV3\text{-}EGFP}$-infected mouse.

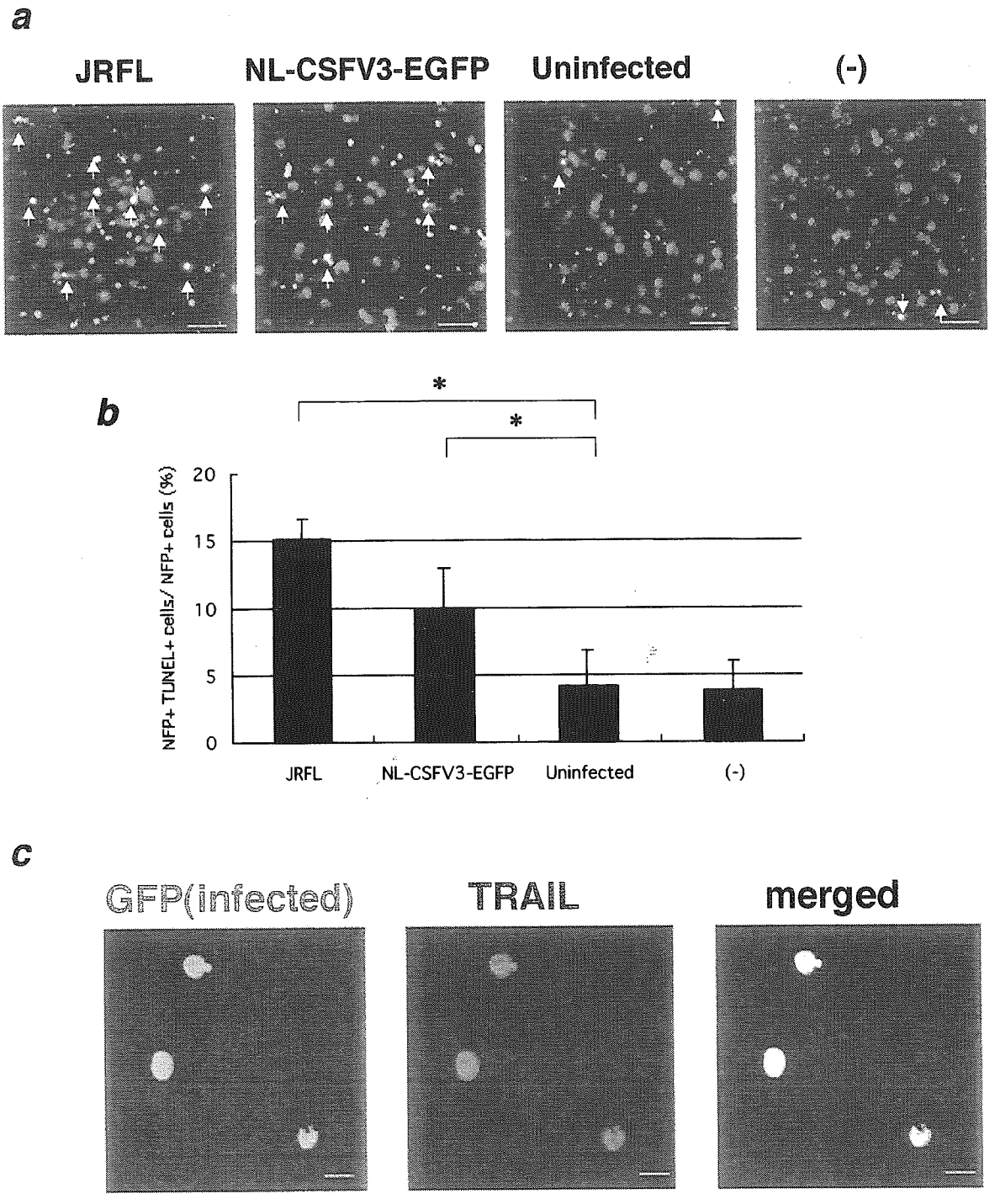

Fig. 3. *In vitro* co-culture system with murine brain cells and HIV-1-infected human MDM. Neurons/glia culture was prepared from fetal mouse brains. Seven days later, HIV-1_{JRFL}-infected, HIV-$1_{NL\text{-}CSFV3\text{-}EGFP}$-infected or uninfected MDM were added to the culture. Four days after co-cultivation, cells were stained. (a) Neuronal apoptosis was evident in neurons/glia cultured with HIV-infected or uninfected human MDM. Apoptotic neurons are identified by the presence of yellow-colored nuclei. Arrows indicate neurofilament protein $(NFP)^+$ $TUNEL^+$ apoptotic neurons. Scale bars = 10 μm. (b) Proportion of apoptotic neurons calculated by counting NFP^+ $TUNEL^+$ cells and total NFP^+ cells. Data are mean $\pm$ SD of triplicate cultures. *, $P < 0.05$ by Student's *t*-test. (c) TRAIL expression in GFP-carrying HIV-infected MDM. Human MDM were isolated from a healthy HIV-1-seronegative donor, cultured and infected with $HIV_{NL\text{-}CSFV3\text{-}EGFP}$ virus. Many GFP^+ HIV-1-infected MDM expressed TRAIL. Scale bars = 20 μm.

3. Induction of neuronal apoptosis co-cultured with HIV-1-infected MDM *in vitro*

To test whether HIV-1-infected macrophages can induce neuronal apoptosis, cultures of primary neurons/glia mixture isolated from fetal mice were established and then co-cultured with HIV-1-infected human MDM. In these experiments, apoptotic neurons were identified by dual-immunostaining for NFP and TUNEL. The numbers of NFP^+ $TUNEL^+$ apoptotic neurons were significantly higher in co-cultures of HIV_{JRFL}- and $HIV_{NL\text{-}CSFV3\text{-}EGFP}$-infected human MDM than in uninfected MDM and cultures of primary neurons/glia cell mixtures (Fig. 3a, b). Furthermore, cultured GFP^+ $HIV_{NL\text{-}CSFV3\text{-}EGFP}$-infected MDM expressed high levels of TRAIL molecule (Fig. 3c). These results suggested that HIV-1-infected human MDM could efficiently induce apoptosis of mouse neurons through a TRAIL-dependent signal pathway *in vitro*.

4. TRAIL induces neuronal apoptosis *in vitro*

To test whether the TRAIL molecule contributes to the induction of apoptosis of neurons, cultures of mouse primary neurons/glia were incubated with human TRAIL-transfected mouse B cell lymphoma cells, 2PK-3. For comparison, cultures of mouse primary neurons/glia were also co-cultured with human FasL-expressing 2PK-3 cells. Overexpression of TRAIL or FasL on the cells was confirmed by FACS analysis (data not shown). Apoptotic neurons were identified by dual staining as described above. The number of NFP^+ $TUNEL^+$ apoptotic neurons was significantly higher in cultures containing human TRAIL-overexpressing cells than human FasL-overexpressing cells or mock-transfected cells (Fig. 4). These results indicated that human TRAIL is important to induce neuronal apoptosis *in vitro*.

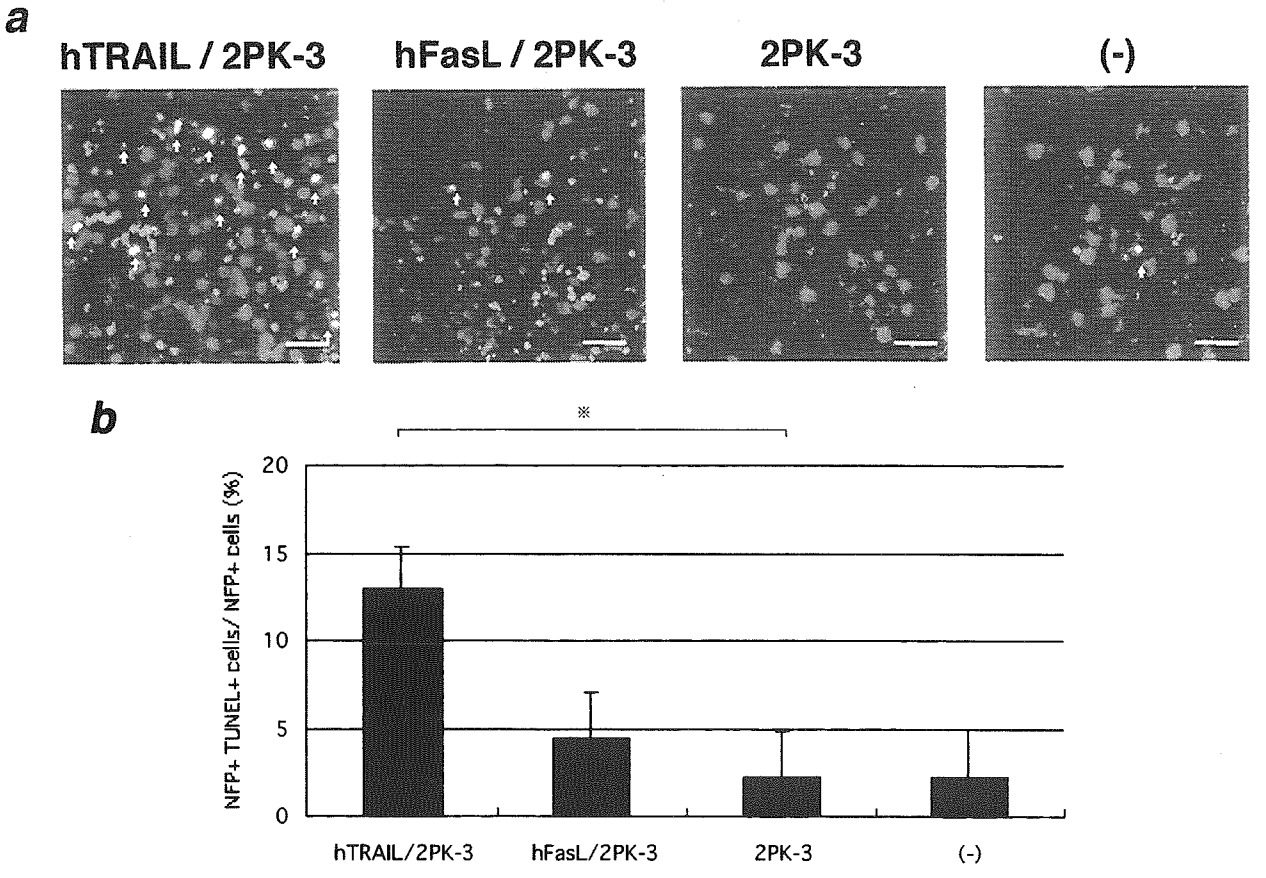

Fig. 4. Neuronal apoptosis of murine neurons/glia co-cultured with TRAIL-transfectant *in vitro*. Primary neurons/glia were co-cultured with human TRAIL/2PK-3, human FasL/2PK-3, or 2PK-3 cells for 4 days. The cells were then immunostained simultaneously with anti-NFP mAb and TUNEL. (a) NFP^+ neurons are shown in red. Nuclei of apoptotic cells are shown in green. Arrows indicate apoptotic neurons with a red cytoplasm and a yellow nucleus (merging of green with red). Scale bars = 10 μm. (b) The proportion of apoptotic neurons was calculated as described above. Data are mean ± SD of triplicate cultures. ※, $P < 0.05$ by Student's *t*-test.

Discussion

1. Role of TRAIL in the brain

In this study, we found significant numbers of TRAIL-expressing cells in the autopsy brains of patients with HIV-encephalopathy and in those of HIV-1-infected hu-PBMC-NOD-SCID mice. *In vitro* experiments of infected macrophages indicated that HIV-1 infection augmented the TRAIL expression. TRAIL expression in the brain tissue has not yet been examined because this molecule has only been recently identified[5]. The TRAIL molecule is a death ligand, however, its pathological role has not been fully examined. Previous studies indicated that TRAIL expression is upregulated by ischemia in the rat brain[20]. In another study[21], injection of a TRAIL antagonist induced exacerbation of experimental allergic encephalomyelitis although no TRAIL-expressing cells were demonstrated in these experiments. On the other hand, Nitsch *et al.*[22] reported induction of apoptosis of cultured human brain cells following the addition of soluble TRAIL. More recently, Dorr and colleagues[23] identified the expression of apoptosis-mediating TRAIL receptors on human neurons. Our results add further support to the importance of TRAIL as a key mediator of apoptosis in the brain, especially in HIV-encephalopathy.

2. Caspase-mediated neuronal apoptosis

There is sufficient evidence for the role of caspase-3 in neuronal apoptosis in the brains of patients with HIV-encephalopathy[24,25]. In particular, significantly high levels of the active form of caspase-3 were found in children with HIV-encephalopathy[26], suggesting that either death ligand-mediated or mitochondria-mediated apoptosis occurs in infected brains. In the present study, we identified activation of caspase-8 in brains of our HIV-encephalopathy patients. Caspase-8 is an earlier mediator of the death pathway and is activated through the TNF receptor family molecules. Apoptosis of neurons cultured with HIV-1 Vpr protein is mediated through caspase-8 activation[27], while activation of caspase-8 has not yet been confirmed in the brain of patients with HIV-encephalopathy. In other CNS diseases, activation of caspase-8 in neurons was reported *in vitro* in reovirus-infections[28], Alzheimer disease[29], prion disease[30], Huntington disease[31], and *in vivo* in ischemic brain[32], Down syndrome[33], Parkinson disease[34], and amyotrophic lateral sclerosis[35].

3. HIV-encephalopathy *in vivo* and *in vitro*-murine system

Our *in vivo* mouse model with HIV-1-systemic infection developed neuronal apoptosis, which was similar to that described in patients with HIV-encephalopathy. Persidsky *et al.*[26] described a HIV-encephalopathy murine model established by intracranial inoculation of HIV-1-infected MDM. In comparison with their model, our mouse model closely resembles HIV-encephalopathy in human because it involves the induction of HIV-1 systemic infection and no artificial trauma of the brain. Using our model, it is possible to examine the mechanism of transmigration of infected cells and systemic neuronal apoptosis in CNS. Our data suggest that transmigration of HIV-1-infected macrophages is induced by certain stimuli and that neuronal apoptosis is augmented by the TRAIL signal on HIV-infected macrophages without infection of murine cells.

We also used a unique *in vitro* human and mouse co-culture system. Since HIV infects only human cells but not murine cells, this is a suitable system to examine the indirect effect of HIV infection. However, it is necessary to consider that human molecules may influence murine cell function, which may limit the use of this system.

4. Infection of macrophages

Our histopathological studies of autopsy brain samples of patients with HIV-dementia indicated that HIV-1 producing cells were limited to monocyte/macrophage lineage. Several studies have suggested that virus-infected macrophages play critical roles in the pathogenesis of encephalopathy and dementia[37]. Recent studies of simian immunodeficiency virus (SIV)-infected animals showed the presence of infiltrating blood-derived, virus-containing macrophages in the perivascular regions and indicated that these pathological changes were seen in all animals with encephalopathy[38]. We extended these results in the present study by demonstrating that the infiltrated macrophages might provide TRAIL signal for neuronal apoptosis.

In conclusion, we have demonstrated in the present study that TRAIL expressed on human macrophages could induce neuronal apoptosis *in vitro*. Since both apoptotic neurons and TRAIL-expressing macrophages were observed *in vivo* in brains of patients with HIV-encephalopathy and in our murine model, a similar mechanism may be involved in the pathogenesis of HIV-encephalopathy. These results provide a strong evidence for the involvement of TRAIL expressed on

HIV-infected macrophages in induction of apoptosis of neurons of HIV-infected brain both *in vitro* and *in vivo*.

Acknowledgments

We thank Professor N. Yamamoto (Department of Molecular Virology, Graduate School, Tokyo Medical and Dental University) for the helpful discussion, Professor K. Inoue (Department of Neurology, Faculty of Medicine, University of Tokyo, presently at Jikei Medical School of Medicine) for kindly providing the human brain specimens, and H. Yagita (Department of Immunology, Juntendo University School of Medicine) for kindly providing 2PK-3 cells. We also thank Dr. F.G. Issa (Word-Medex) for the careful reading and editing of the manuscript.

References

1. Funata N, Maeda Y, Koike M et al. Neuropathology of the central nervous system in acquired immune deficiency syndrome (AIDS) in Japan with special reference to human immunodeficiency virus-induced encephalomyelopathies. Acta Pathol Jpn 1991;41:206-11.
2. Schindelmeiser J, Gullotta F. HIV-p24-antigen-bearing macrophages are only present in brains of HIV-seropositive patients with AIDS-encephalopathy. Clin Neuropathol 1991;10:109-11.
3. Kaul M, Garden G A, Lipton S A. Pathways to neuronal injury and apoptosis in HIV-associated dementia. Nature 2001;410:988-94.
4. Shi B, De Girolami U, He J et al. Apoptosis induced by HIV-1 infection of the central nervous system. J Clin Invest 1996;98:1979-90.
5. Wiley S R, Schooley K, Smolak P J et al. Identification and characterization of a new member of the TNF family that induces apoptosis. Immunity 1995;3:673-82.
6. Srivastava R K. TRAIL/Apo-2L: mechanisms and clinical applications in cancer. Neoplasia 2001;3:535-46.
7. Wu G S, Burns T F, Zhan Y et al. Molecular cloning and functional analysis of the mouse homologue of the KILLER/DR5 tumor necrosis factor-related apoptosis-inducing ligand (TRAIL) death receptor. Cancer Res 1999;59:2770-5.
8. Wajant H, Pfizenmaier K, Scheurich P. TNF-related apoptosis inducing ligand (TRAIL) and its receptors in tumor surveillance and cancer therapy. Apoptosis 2002;7:449-59.
9. Clarke P, Meintzer S M, Gibson S et al. Reovirus-induced apoptosis is mediated by TRAIL. J Virol 2000;74:8135-9.
10. Vidalain P O, Azocar O, Lamouille B et al. Measles virus induces functional TRAIL production by human dendritic cells. J Virol 2000;74:556-9.
11. Miura Y, Misawa N, Maeda N et al. Critical contribution of tumor necrosis factor-related apoptosis-inducing ligand (TRAIL) to apoptosis of human CD4+ T cells in HIV-1-infected hu-PBL-NOD-SCID mice. J Exp Med 2001;193:651-60.
12. Koyanagi Y, Miles S, Mitsuyasu R T et al. Dual infection of the central nervous system by AIDS viruses with distinct cellular tropisms. Science 1987;236:819-22.
13. Murphy T H, Baraban J M, Wier W G. Mapping miniature synaptic currents to single synapses using calcium imaging reveals heterogeneity in postsynaptic output. Neuron 1995;15:159-68.
14. Kayagaki N, Yamaguchi N, Nakayama M et al. Involvement of TNF-related apoptosis-inducing ligand in human CD4+ T cell-mediated cytotoxicity. J Immunol 1999;162:2639-47.
15. Quinn B, Toga A W, Motamed S et al. Fluoro nissl green: a novel fluorescent counterstain for neuroanatomy. Neurosci Lett 1995;184:169-72.
16. Zhang M, Li X, Pang X et al. Identification of a potential HIV-induced source of bystander-mediated apoptosis in T cells: upregulation of trail in primary human macrophages by HIV-1 tat. J Biomed Sci 2001;8:290-6.
17. Liabakk N B, Sundan A, Torp S et al. Development, characterization and use of monoclonal antibodies against sTRAIL: measurement of sTRAIL by ELISA. J Immunol Methods 2002;259:119-28.
18. Ng Y K, Ling E A. Induction of major histocompatibility class II antigen on microglial cells in postnatal and adult rats following intraperitoneal injections of lipopolysaccharide. Neurosci Res 1997;28:111-8.
19. Nottet H S, Persidsky Y, Sasseville V G et al. Mechanisms for the transendothelial migration of HIV-1-infected monocytes into brain. J Immunol 1996;156:1284-95.
20. Martin-Villalba A, Herr I, Jeremias I et al. CD95 ligand (Fas-L/APO-1L) and tumor necrosis factor-related apoptosis-inducing ligand mediate ischemia-induced apoptosis in neurons. J Neurosci 1999;19:3809-17.
21. Hilliard B, Wilmen A, Seidel C et al. Roles of TNF-related apoptosis-inducing ligand in experimental autoimmune encephalomyelitis. J Immunol 2001;166:1314-9.
22. Nitsch R, Bechmann I, Deisz R A et al. Human brain-cell death induced by tumour-necrosis-factor-related apoptosis-inducing ligand (TRAIL). Lancet 2000;356:827-8.
23. Dorr J, Bechmann I, Waiczies S et al. Lack of tumor necrosis factor-related apoptosis-inducing ligand but presence of its receptors in the human brain. J Neurosci 2002;22:RC209.
24. Zheng J, Thylin M R, Ghorpade A et al. Intracellular CXCR4 signaling, neuronal apoptosis and neuropathogenic mechanisms of HIV-1-associated dementia. J Neuroimmunol 1999;98:185-200.
25. Garden G A, Budd S L, Tsai E et al. Caspase cascades in human immunodeficiency virus-associated neurodegeneration. J Neurosci 2002;22:4015-24.
26. James H J, Sharer L R, Zhang Q et al. Expression of caspase-3 in brains from paediatric patients with HIV-1 encephalitis. Neuropathol Appl Neurobiol 1999;25:380-6.
27. Patel C A, Mukhtar M, Pomerantz R J. Human immunodeficiency virus type 1 Vpr induces apoptosis in human neuronal cells. J Virol 2000;74:9717-26.
28. Richardson-Burns S M, Kominsky D J, Tyler K L. Reovirus-induced neuronal apoptosis is mediated by caspase 3 and is associated with the activation of death receptors. J Neurovirol 2002;8:365-80.
29. Wei W, Norton DD, Wang X et al. Abeta 17-42 in Alzheimer's disease activates JNK and caspase-8 leading to neuronal apoptosis. Brain 2002;125:2036-43.
30. White A R, Guirguis R, Brazier M W et al. Sublethal concentrations of prion peptide PrP106-126 or the amyloid beta peptide of Alzheimer's disease activates expression of proapoptotic markers in primary cortical neurons. Neurobiol Dis 2001;8:299-316.
31. Gervais F G, Singaraja R, Xanthoudakis S et al. Recruitment

and activation of caspase-8 by the Huntingtin-interacting protein Hip-1 and a novel partner Hippi. Nat Cell Biol 2002;4:95-105.
32. Yin X M, Luo Y, Cao G et al. Bid-mediated Mitochondrial Pathway Is Critical to Ischemic Neuronal Apoptosis and Focal Cerebral Ischemia. J Biol Chem 2002;277:42074-81.
33. Gulesserian T, Engidawork E, Yoo B C et al. Alteration of caspases and other apoptosis regulatory proteins in Down syndrome. J Neural Transm 2001;61(Suppl):163-79.
34. Hartmann A, Troadec J D, Hunot S et al. Caspase-8 is an effector in apoptotic death of dopaminergic neurons in Parkinson's disease, but pathway inhibition results in neuronal necrosis. J Neurosci 2001;21:2247-55.
35. Raoul C, Estevez AG, Nishimune H et al. Motoneuron death triggered by a specific pathway downstream of Fas. potentiation by ALS-linked SOD1 mutations. Neuron 2002;35:1067-83.
36. Persidsky Y, Limoges J, McComb R et al. Human immunodeficiency virus encephalitis in SCID mice. Am J Pathol 1996;149:1027-53.
37. Balestra E, Perno CF, Aquaro S et al. Macrophages: a crucial reservoir for human immunodeficiency virus in the body. J Biol Regul Homeost Agents 2001;15:272-6.
38. Williams K C, Corey S, Westmoreland S V et al. Perivascular macrophages are the primary cell type productively infected by simian immunodeficiency virus in the brains of macaques: implications for the neuropathogenesis of AIDS. J Exp Med 2001;193:905-15.

Tumor necrosis factor-related apoptosis-inducing ligand induces neuronal death in a murine model of HIV central nervous system infection

Yoshiharu Miura*†, Naoko Misawa*, Yuji Kawano*, Hiroshi Okada*, Yoshio Inagaki‡, Naoki Yamamoto‡, Mamoru Ito§, Hideo Yagita¶, Ko Okumura¶, Hidehiro Mizusawa†‖, and Yoshio Koyanagi*‖

*Department of Virology, Tohoku University Graduate School of Medicine, Sendai 980-8575, Japan; Departments of †Neurology and Neurological Science and ‡Molecular Virology, Tokyo Medical and Dental University, Tokyo 113-8519, Japan; §Central Institute for Experimental Animals, Kawasaki 216-0001, Japan; and ¶Department of Immunology, Juntendo University School of Medicine, Tokyo 113-8421, Japan

Communicated by Leonard A. Herzenberg, Stanford University School of Medicine, Stanford, CA, December 27, 2002 (received for review December 11, 2002)

HIV-1 infection in the brain induces neuronal apoptosis leading to HIV-associated dementia. To explore the underlying mechanism, we developed a murine model by using human peripheral blood mononuclear cell (PBMC)–transplanted nonobese diabetic (NOD)–severe combined immunodeficiency (SCID) (hu-PBMC-NOD-SCID) mice. Administration of lipopolysaccharide (LPS) to HIV-1-infected hu-PBMC-NOD-SCID mice induced infiltration of HIV-1-infected human cells into the perivascular region of the brain and neuronal apoptosis was found in macrophage (M)-tropic but not T cell (T)-tropic HIV-1-infected brains. The apoptotic neurons were frequently colocalized with the HIV-1-infected macrophages that expressed tumor necrosis factor (TNF)-related apoptosis-inducing ligand (TRAIL). Administration of a neutralizing antibody against human TRAIL but not human TNF-α or Fas ligand (FasL) blocked the neuronal apoptosis in the HIV-1-infected brain. These results strongly suggest a critical contribution of TRAIL expressed on HIV-1-infected macrophages to neuronal apoptosis.

HIV-1 infection in the brain induces a neuropathology, termed HIV encephalopathy, that is characterized by astrocytosis, microglial nodules, cell infiltration with macrophages, decreased synaptic density, and selective neuronal loss (1). These neurodegenerative changes result in cognitive and motor dysfunction, designated HIV-associated dementia. The neuronal damage is caused by apoptosis, as demonstrated histologically in brains from HIV encephalopathy patients (2) and experimentally by *in vitro* infection with HIV-1 (3). HIV-1 infects macrophages and microglia but not neurons in the infected brain, suggesting an indirect mechanism for HIV-1-induced neuronal apoptosis (4). A critical contribution of neurotoxic substances released from the infected and/or activated macrophages/microglia, including excitatory amino acids, IL-1β, and tumor necrosis factor (TNF)-α, to neuronal apoptosis has been suggested through *in vitro* studies (5, 6). However, the precise mechanism for HIV-induced neuronal apoptosis *in vivo* has not been elucidated yet because of the lack of an appropriate animal model. Although the neuropathogenesis of simian immunodeficiency virus (SIV) or chimeric simian/HIV (SHIV) in a monkey model has been reported, the molecular mechanism leading to neuronal apoptosis *in vivo* has not been clarified (7, 8). We developed an HIV-1-susceptible mouse model by using human peripheral blood mononuclear cell (PBMC)–transplanted nonobese diabetic (NOD)–severe combined immunodeficiency (SCID) (hu-PBMC-NOD-SCID) mice (9). When infected with either macrophage (M)-tropic or T cell (T)-tropic HIV-1, a systemic infection with high levels of viremia, which led to a progressive $CD4^+$ T cell loss, was reproducibly established in these mice. Using this mouse model, we recently demonstrated a critical contribution of TRAIL to the depletion of HIV-1-uninfected bystander $CD4^+$ T cells in lymphoid organs that is largely responsible for the pathogenesis of AIDS (10). In the present study, we developed a mouse model that HIV-1 infection extended to central nervous system (CNS). Intraperitoneal administration of LPS to the M-tropic HIV-1-infected hu-PBMC-NOD-SCID mice induced a neuropathology that resembled part of the HIV encephalopathy of human patients, including infiltration of HIV-infected macrophages, astrocytosis, and neuronal apoptosis in the brain. Using this model, we demonstrated a critical contribution of TRAIL to the HIV-1-induced neuronal apoptosis.

Materials and Methods

Reconstitution and HIV-1 Infection of hu-PBMC-NOD-SCID Mice. NOD (NOD/Shi) *scid/scid* (NOD-SCID) mice were used at 6–8 weeks of age. The experimental protocol was approved by the Ethics Review Committee for Animal Experimentation of the participating institutions. Reconstitution with human PBMCs and infection with HIV-1 were performed as described (9). Briefly, human PBMCs were isolated from a healthy HIV-1-seronegative donor and injected i.p. Five days later, mice were inoculated i.p. with 1,000 ID_{50} of JRFL HIV-1 isolate (11), 100,000 ID_{50} of NL4-3 (12), or recombinant HIV-1 expressing green fluorescent protein (GFP). The T-tropic HIV-1 expressing GFP (NL-EGFP) was constructed from NL4-3 by inserting an enhanced GFP (*EGFP*) gene and an *internal ribosome entry site* (*IRES*) sequence between gp41 and the *nef* sequence by PCR-based subcloning. The ATG codon of *EGFP* was placed 2 bp downstream of gp41 termination codon and *nef* expression was rescued from insertion of the *IRES* sequence. The M-tropic HIV-1 expressing GFP (NL-CSFV3-EGFP) was constructed by replacing the V3 sequence in the NL-EGFP with the V3 sequence from JRCSF (11). One hundred micrograms of LPS (Sigma) was injected i.p. 7 days after HIV-1 inoculation. Three or 21 days later, the brains were fixed in 4% periodate-lysine-paraformaldehyde (PLP) fixative. The brains were cut into four serial coronal sections at the level of corpus callosum, hippocampus, and cerebellum. Then they were subjected to immunohistological analyses.

Administration of mAbs. One milligram of anti-human TRAIL mAb (clone RIK-2, IgG; ref. 13), anti-human Fas ligand (FasL) mAb (clone NOK-1, IgG; ref. 14), anti-human TNF-α mAb (clone 28401.111, Genzyme/Techne, Minneapolis), or a control mouse IgG (Inter-Cell Technologies, Hopewell, NJ) was administered i.p. at the time of the LPS injection. The mice were killed

Abbreviations: cps, cells per slice; EGFP, enhanced GFP; FNG, FluoroNissl Green; $cFNG^+$, cytoplasmic FNG^+; FasL, Fas ligand; LPS, lipopolysaccharide; M-tropic, macrophage-tropic; PBMC, peripheral blood mononuclear cell; hu-PBMC-NOD-SCID, human PBMC–transplanted nonobese diabetic–severe combined immunodeficiency; TNF, tumor necrosis factor; TRAIL, TNF-related apoptosis-inducing ligand; T-tropic, T cell-tropic; TUNEL, terminal deoxynucleotidyl transferase-mediated dUTP nick-end labeling.

‖To whom correspondence may be addressed. E-mail: koyanagi@mail.cc.tohoku.ac.jp or h-mizusawa.nuro@tmd.ac.jp.

Table 1. HIV-CNS infection and apoptosis in HIV-infected hu-PBMC-NOD-SCID mice

PBMC	Virus	LPS	*n*	Brain							Peritoneal space, HLA$^+$ ($\times 10^4$ cells)[§]
				CD3$^+$	CD68$^+$	p24^{+*}	TUNEL$^+$	cFNG$^+$ TUNEL$^+$	AC[†]	MN[‡]	
+	JRFL	−	5	24.4 ± 14.4[¶]	NDe	10.2 ± 7.69[¶]	11.4 ± 5.37[¶]	NDe	±	−	213.2 ± 159.7[¶]
+	None	−	5	21.6 ± 12.3	NDe	NT	7.50 ± 1.48	NDe	±	−	462.9 ± 77.3
−	None	−	4	NT	NT	NT	NDe	NDe	−	−	NT
+	JRFL	+	12	91.3 ± 34.4[¶]	21.3 ± 5.31	58.4 ± 21.5[¶]	78.8 ± 21.5[¶]	13.1 ± 4.47	+	+	47.1 ± 37.2[¶]
+	None	+	6	37.0 ± 27.4	13.0 ± 4.98	NT	25.0 ± 10.8	NDe	+	+	157.7 ± 98.4
−	None	+	5	NT	NT	NT	NDe	NDe	+	+	NT
+	NL4-3	−	4	30.0 ± 19.7	NDe	7.25 ± 4.57	10.0 ± 4.24	NDe	±	−	125.2 ± 69.6
+	NL4-3	+	4	36.0 ± 12.7	13.0 ± 4.16	26.8 ± 7.46	33.3 ± 9.36	NDe	+	+	18.2 ± 15.6
+	NL-CSFV3-EGFP	+	5	74.8 ± 63.2	18.8 ± 10.4	45.4 ± 32.6	56.4 ± 8.32	10.8 ± 4.97	+	+	77.3 ± 67.4
+	NL-EGFP	+	5	33.0 ± 20.7	10.2 ± 2.39	22.2 ± 7.95	31.4 ± 9.86	NDe	+	+	65.8 ± 43.9

hu-PBMC-NOD-SCID mice were infected with the indicated strains of HIV-1, and LPS was given 7 days after infection. Three days later, mice were sacrificed and brains were subjected to immunohistological staining. Numbers of human CD3$^+$, human CD68$^+$, HIV gag p24$^+$, TUNEL$^+$, and TUNEL$^+$ cytoplasmic FluoroNissl Green (cFNG)$^+$ cells per slice are indicated as the mean ± SD. Four to 12 mice in each group. NDe, not detected; NT, not tested.

*Number of p24$^+$ cells was almost similar to that of GFP$^+$ cells.

[†]AC, astrocytosis; +, significant proliferation of sharp GFAP$^+$ cells; ±, slight proliferation of GFAP$^+$ cells; −, no proliferation.

[‡]MN, microglial nodule.

[§]Numbers of HLA-ABC$^+$ cells in mouse peritoneal lavage.

[¶]$P < 0.05$ compared by Welch's *t* test between untreated and LPS-treated mice with JRFL infection.

3 days later, and the brains were subjected to histological analyses.

Immunohistological Staining. Abs against the following molecules were used for PLP fixed section as primary Abs: human CD3 (rabbit polyclonal IgG, Dako), human CD68 (clone PGM1, mouse monoclonal IgG, Dako), glial fibrillary acidic protein (GFAP) (rabbit polyclonal IgG, Dako), HIV-1 gag p24 (clone Kal-1, mouse monoclonal IgG, Dako), and mouse F4/80 (clone F4/80, rat monoclonal IgG, Serotec). Detection of the immunohistological staining was performed as described (10). Nonimmunized rabbit, mouse, and rat Ig (Dako) were used as negative controls. Terminal deoxynucleotidyl transferase (TdT)-mediated dUTP nick-end labeling (TUNEL) staining of frozen sections was carried out using an indirect method as described (10). Absence of either digoxigenin-labeled dUTP or TdT served as a negative control. DNase-treated sections served as positive controls.

Frozen sections were incubated with Abs against human CD68 (clone PGM1), human TRAIL (clone RIK-2), IL-1β (rabbit polyclonal IgG, Endogen, Woburn, MA), human TNF-α (rabbit polyclonal IgG, Endogen), human FasL (rabbit polyclonal IgG, Santa Cruz Biotechnology), HIV-1 gag p24 (goat polyclonal IgG, ViroStat, Portland, ME), or the active form of caspase-3 (rabbit polyclonal IgG, R & D Systems). The sections were then incubated with FITC-conjugated secondary Abs as described (10). Dual-color staining, including TUNEL, was performed FluoroNissl Green (FNG, FMP) (15), NeuroTrace blue fluorescent Nissl stain (FNB, FMP), or anti-microtubule-associated protein (MAP)-2 mAb (clone HM-2, mouse monoclonal IgG, Sigma). HIV gag p24 (Kal-1, Dako) and human CD68 (PGM1, Dako) were also used. Secondary Abs were used as described (10). Triple-color analysis for GFP, CD68, and TRAIL, TNF-α, or FasL was also performed as described (10). An absence of primary Ab was used as a negative control. Sections were covered with Vector Shield mounting medium (Vector Laboratories) and observed under a Zeiss LSM 310 confocal laser-scanning microscope.

Serial coronal sections (at least three slices) were scored for the immunostained cells by a single investigator in a blinded manner. All over the sections were evaluated in each sample. Apoptotic cells were also identified using active form of caspase-3 staining and hematoxylin/eosin (H&E) staining. Cells undergoing apoptosis were identified by characteristic morphology including nuclear fragmentation and cell shrinkage with condensed nuclei on H&E-stained sections. In dual-color detection of GFP and human CD3 or CD68, the percentage of double-positive cells was calculated. In dual-color staining of CD68 or CD3 and TNF-α, IL-1β, TRAIL, or FasL, the percentage of double-positive cells in CD68$^+$ or CD3$^+$ cells was calculated.

Statistics. Data are presented as the mean ± SD of slices. Welch's *t* test was used to compare the mean values between two groups. *P* values <0.05 were regarded as statistically significant.

Results

Development and Characterization of an HIV-CNS Infection Model. It has been proposed that HIV infection in the brain is initiated by the migration of M-tropic HIV-infected macrophages (16). Thus, we first examined the migration of HIV-infected human PBMCs into the brain of hu-PBMC-NOD-SCID mice after infection with a M-tropic JRFL or a T-tropic NL4-3 virus. Low levels of human CD3$^+$ T cell migration [24.4 ± 14.4 cells per slice (cps) in JRFL-infected brains and 30.0 ± 19.7 cps in NL4-3-infected brains] and, less frequently, HIV gag p24$^+$ cell migration (10.2 ± 7.69 cps in JRFL-infected brains and 7.25 ± 4.57 cps in NL4-3-infected brains), but not human CD68$^+$ macrophages, were found in the meninx and around the vessel of the brain 10 days after infection (Table 1). Because we observed similar levels of CD3$^+$ T cell migration in mice 28 days after infection (data not shown) and in brains from uninfected mice (21.6 ± 12.3 cps, Table 1), these data appear to represent the baseline distribution of T cells and macrophages in hu-PBMC-NOD-SCID mice. We observed no apparent neuropathology excepting sparse astrocytosis in the brains of infected mice (data not shown).

To facilitate the migration of HIV-infected macrophages into the brain, we administered a sublethal dose of LPS (100 μg) i.p. to the JRFL- or NL4-3-infected hu-PBMC-NOD-SCID mice 7 days after infection, because LPS has been reported to enhance the transendothelial migration of macrophages and T cells into the brain through its activation (17). A marked increase in human CD68$^+$ macrophages (21.3 ± 5.3 cps in JRFL-infected brains and 13.0 ± 4.16 cps in NL4-3-infected brains) and HIV gag p24$^+$ cells (58.4 ± 21.5 cps in JRFL-infected brains and 26.8 ± 7.46 cps in NL4-3-infected brains), as well as human